ARTICLE

doi:10.1038/nature25463

# Teneurin-3 controls topographic circuit assembly in the hippocampus

Dominic S. Berns[1,2,3], Laura A. DeNardo[1,2], Daniel T. Pederick[1,2] & Liqun Luo[1,2]

**Brain functions rely on specific patterns of connectivity. Teneurins are evolutionarily conserved transmembrane proteins that instruct synaptic partner matching in *Drosophila* and are required for vertebrate visual system development. The roles of vertebrate teneurins in connectivity beyond the visual system remain largely unknown and their mechanisms of action have not been demonstrated. Here we show that mouse teneurin-3 is expressed in multiple topographically interconnected areas of the hippocampal region, including proximal CA1, distal subiculum, and medial entorhinal cortex. Viral-genetic analyses reveal that teneurin-3 is required in both CA1 and subicular neurons for the precise targeting of proximal CA1 axons to distal subiculum. Furthermore, teneurin-3 promotes homophilic adhesion *in vitro* in a splicing isoform-dependent manner. These findings demonstrate striking genetic heterogeneity across multiple hippocampal areas and suggest that teneurin-3 may orchestrate the assembly of a complex distributed circuit in the mammalian brain via matching expression and homophilic attraction.**

The hippocampal region is critical for the acquisition of declarative memory and the neural representation of space[1–4]. The connections between hippocampal subregions and adjacent cortex are topographically organized along both the dorsal–ventral and proximal–distal axes[5]. Along the proximal–distal axis, proximal CA1, distal subiculum, and medial entorhinal cortex (MEC) neurons are specifically interconnected, as are distal CA1, proximal subiculum, and lateral entorhinal cortex (LEC) neurons[6,7]. These two parallel circuits may be preferentially used for processing spatial and object-related information, respectively[8]. Genetic heterogeneity that could contribute to the observed anatomical and functional differentiation along the proximal–distal axis in CA1 has been reported[9]. However, the mechanisms that control the exquisite wiring specificity remain unknown.

Since the proposal of the chemoaffinity hypothesis for establishing specific neuronal connections[10], many cell surface and secreted proteins have been discovered that guide developing axons to target regions and recognize specific synaptic partners[11,12]. Members of the teneurin family of type II transmembrane proteins exhibit matching expression in pre- and postsynaptic partners and instruct synaptic partner choice in the *Drosophila* olfactory and neuromuscular systems, probably through homophilic attraction[13,14]. Teneurins are evolutionarily conserved, with four members in mammals[15] that are dynamically expressed during brain development[16]. Human teneurins are risk loci in bipolar disorder[17–20] and schizophrenia[21], and are implicated in other neurological disorders[22,23]. Teneurin-3 (Ten3) is required for proper dendrite morphogenesis and axon targeting in the vertebrate visual system[24–27]. Although Ten3 has been hypothesized to function as a homophilic attractant, no cellular or molecular mechanisms have been demonstrated. Furthermore, conflicting evidence exists as to whether vertebrate teneurins interact in *trans* in a homophilic manner[28–30], and heterophilic *trans* interactions with the adhesion-type G-protein-coupled receptors latrophilins have been demonstrated[30–32]. Here, we examine the role of Ten3 in the development of specific connections within the hippocampal region, and shed new light on its mechanism of action during mammalian neural development.

## Ten3 expression in hippocampal regions

Using a custom antibody against a cytoplasmic epitope (Extended Data Fig. 1a), we found that Ten3 was expressed in highly specific regions of the postnatal brain. In particular, Ten3 was expressed in restricted domains of the developing hippocampal region (Fig. 1a), including proximal CA1, distal subiculum, and MEC. A second Ten3 antibody against an extracellular epitope recapitulated this staining pattern (Extended Data Fig. 1a, d). Staining with both antibodies was abolished in *Ten3* knockout mice ($Ten3^{\Delta 4/\Delta 4}$)[24] (Extended Data Fig. 1b–e). Ten3 was most prominent in synaptic layers, including stratum lacunosum-moleculare of CA1 and the molecular layer of subiculum, consistent with Ten3 being present in the synaptic cleft[33]. Ten3 was also present in axons, dendrites, and cell bodies (Extended Data Fig. 1f–i). *In situ* hybridization revealed that *Ten3* mRNA was expressed in all regions where Ten3 protein was observed (Fig. 1b and Extended Data Fig. 1j). In both CA1 and subiculum, *Ten3* mRNA showed a graded distribution along the proximal–distal axis, peaking in proximal CA1 and distal subiculum (Fig. 1c and Extended Data Fig. 2).

Remarkably, Ten3 protein and mRNA expression patterns corresponded to the known topography of multiple connections in the hippocampal region. MEC neurons send axons to proximal CA1 and distal subiculum[34–36], proximal CA1 neurons project to distal subiculum[37,38] and MEC[6,7], and distal subicular neurons project to MEC[6,39]. All of these regions highly expressed Ten3 protein and mRNA (Fig. 1a–c). By contrast, LEC neurons are interconnected with distal CA1 and proximal subiculum[6,7,34–40], all of which expressed low or no Ten3. To further examine the relationship between Ten3 expression and topographic projections, we injected an anterograde viral tracer into MEC, and found that MEC axons and Ten3 protein clearly overlapped in the molecular layers of proximal CA1 and distal subiculum (Fig. 1d). By contrast, LEC axons projected to distal CA1 and proximal subiculum, regions of low Ten3 expression (Fig. 1e).

In summary, Ten3 expression matches with topographic connectivity between entorhinal cortex, CA1, and subiculum (Fig. 1f). Ten3 protein and mRNA were also specifically expressed in subregions of the presubiculum, parasubiculum, medial mammillary nucleus, and anteroventral thalamic nucleus that are topographically connected

[1]Howard Hughes Medical Institute, Stanford University, Stanford, California 94305, USA. [2]Department of Biology, Stanford University, Stanford, California 94305, USA. [3]Neurosciences Graduate Program, Stanford University, Stanford, California 94305, USA.

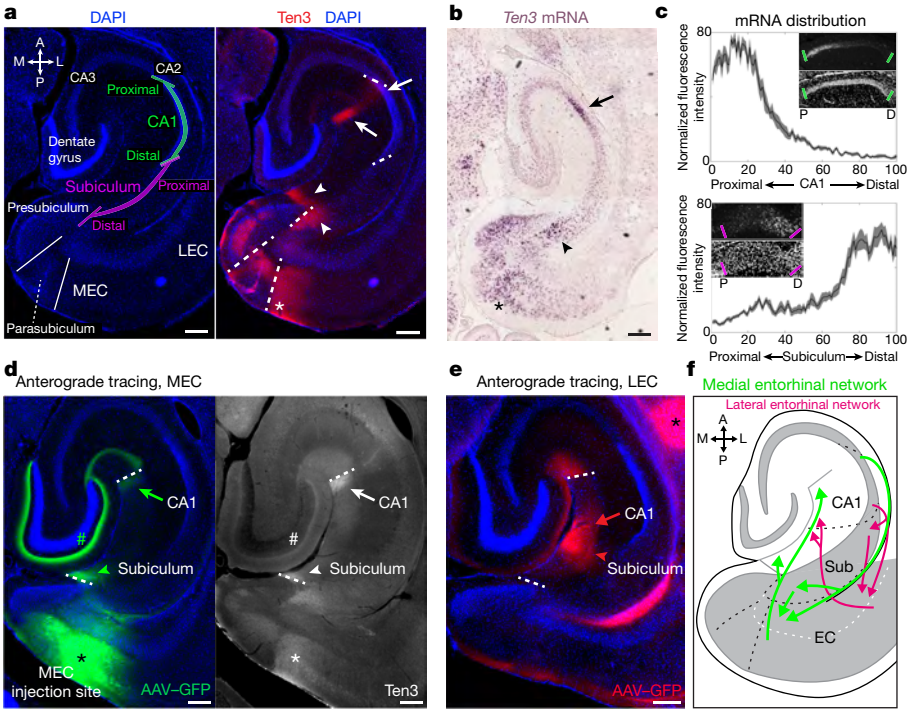


**Figure 1 | Ten3 expression in the developing hippocampal region.** **a**, Left: diagram of the hippocampal region on a horizontal section of P10 mouse brain. A, anterior; P, posterior; M, medial; L, lateral. Right: same section with Ten3 immunostaining. **b**, *In situ* hybridization for *Ten3* mRNA on a P9 horizontal section. In **a** and **b**, arrows denote proximal CA1; arrowheads, distal subiculum; asterisk, MEC. **c**, Quantification of *Ten3* mRNA along the proximal–distal (P–D) axis of CA1 ($n = 12$ sections, four mice) and subiculum ($n = 14$ sections, four mice) of P10 horizontal sections. Insets: *Ten3* mRNA (top) and DAPI (4′,6-diamidino-2-phenylindole) staining (bottom). The *x* axis represents bin along the proximal–distal axis of CA1 or subiculum. Shaded curves, mean ± s.e.m. **d**, Labelling of MEC axons projecting to hippocampus in P70 brain after *AAV1-CMV–GFP* injection in MEC (asterisk) (left) and Ten3 staining on the same section (right). GFP in layer III MEC axons overlaps with Ten3 in proximal CA1 (arrows) and distal subiculum (arrowheads); GFP in layer II MEC axons also overlaps with Ten3 in dentate gyrus (#). **e**, Labelling of LEC axons in P55 brain projecting to distal CA1 (arrow) and proximal subiculum (arrowhead). Asterisk identifies track to the more ventral injection site. **f**, Summary of topographic connections between MEC, proximal CA1, and distal subiculum (Sub) (green arrows), and between LEC, distal CA1, and proximal subiculum (red arrows). Scale bars, 200 μm.

with subiculum or entorhinal cortex (Extended Data Fig. 3). Given the function of *Drosophila* teneurins in synaptic partner matching[13,14], we hypothesized that Ten3 may act as a homophilic attractant to control the development of these precise wiring patterns.

## *Ten3* knockout analysis

To test the function of Ten3 in hippocampal circuit development, we focused on the projection from CA1 to subiculum, where proximal CA1 neurons (Ten3-high) send axons to distal subiculum (Ten3-high), and distal CA1 neurons (Ten3-low) project to proximal subiculum (Ten3-low) (Fig. 2a–c). We generated a *Ten3* knock-in *cre* allele ($Ten3^{cre}$, Extended Data Fig. 4a), which functioned as a protein null and allowed us to visualize neurons that normally express Ten3 in a mutant background (Extended Data Fig. 4b–d). We injected the anterograde tracer *Phaseolus vulgaris* leucoagglutinin (PHA-L)[41] into proximal CA1 of the dorsal hippocampus of *Ten3* heterozygous ($Ten3^{cre/+}$, hereafter $Ten3^{Het}$) and knockout ($Ten3^{cre/\Delta 4}$, hereafter $Ten3^{KO}$) mice, and analysed the distribution of labelled CA1 axons in subiculum (Fig. 2c–g). In $Ten3^{Het}$ mice, proximal CA1-restricted injections labelled axons that arborized densely in distal subiculum, confirming the topography described in the rat[37,38] (Fig. 2c). In $Ten3^{KO}$ mice, however, similarly placed injections in proximal CA1 labelled axons that spread significantly more proximally in subiculum (Fig. 2d, e), with increased overall width (Fig. 2f) and a proximal shift in the mean position (Fig. 2g) of the projection. Middle and distal CA1 injections revealed that the overall topography of the CA1→subiculum projection was less sharp in $Ten3^{KO}$ mice (Extended Data Fig. 5). Thus, Ten3 is required for the precise projections of proximal CA1 axons to distal subiculum.

We next recorded excitatory postsynaptic currents (EPSCs) from proximal and distal subicular cells in hippocampal slices from $Ten3^{+/+}$ ($Ten3^{WT}$) and $Ten3^{KO}$ mice in response to electrical stimulation of the CA1→subiculum axon bundles (Fig. 2h). In $Ten3^{WT}$ slices, stimulation reliably evoked EPSCs in proximal and distal subicular neurons (Fig. 2i). In $Ten3^{KO}$ mice, evoked EPSC amplitudes in distal but not proximal subicular neurons were strongly reduced, consistent with the anatomical defect in $Ten3^{KO}$ mice (Fig. 2i, j). The paired pulse ratio was unaffected in proximal subicular neurons but was increased in distal subicular knockout cells, indicating a lower baseline release probability in *Ten3* mutants (Fig. 2k). Given that, in knockout mice, some proximal CA1 axons still reached distal subiculum (Fig. 2d, e), the marked physiological changes suggest that Ten3 may also be required for formation or function of the synapses between proximal CA1 and distal subicular neurons, consistent with the persistent expression of Ten3 in adults (Fig. 1d) and the function of *Drosophila* teneurins in synapse formation[14,42].

## CA1 conditional knockout analysis

To distinguish whether Ten3 is required in CA1, subiculum, or both, for the CA1→subiculum projection, we generated a conditional *Ten3* allele ($Ten3^{fl}$) that allowed us to delete *Ten3* in cells expressing Cre recombinase (Extended Data Fig. 6). Because the CA1→subiculum projection develops postnatally (Extended Data Fig. 7), we injected cre-expressing lentivirus into either CA1 or subiculum at postnatal day 0 (P0) to generate area-specific *Ten3* knockouts.

For CA1 conditional knockout, we injected a Cre-dependent anterograde tracer into proximal CA1 of adults to visualize axons only from Cre-expressing neurons (Fig. 3a). In $Ten3^{WT}$ controls, proximal CA1

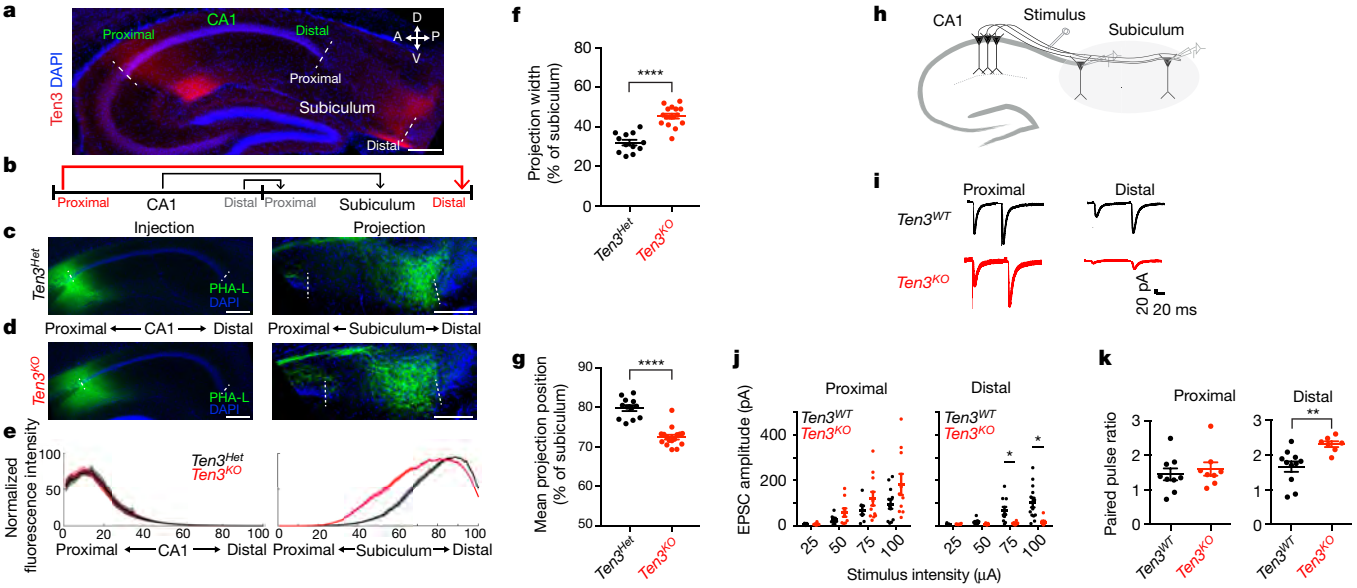


**Figure 2 | Ten3 is required for the precise CA1→subiculum projection.** **a**, Sagittal section of P11 hippocampus, showing Ten3 expression in proximal CA1 and distal subiculum. A, anterior; P, posterior; D, dorsal; V, ventral. **b**, Diagram of the CA1→subiculum topographic projection, with Ten3-high regions and axons in red. **c**, **d**, PHA-L (green) injections in proximal CA1 and corresponding projections in subiculum of $Ten3^{Het}$ (**c**) or $Ten3^{KO}$ (**d**) mice. **e**, Averaged normalized fluorescence intensity traces for proximal injections in CA1 (left) and corresponding projections in subiculum (right) for $Ten3^{Het}$ (black, $n = 12$ mice) and $Ten3^{KO}$ (red, $n = 16$ mice). The *x* axis represents bin along the proximal–distal axis of CA1 or subiculum. Shaded curves represent mean ± s.e.m. at each bin. **f**, **g**, Projection width-at-half-maximum (**f**) and mean position (**g**) for $Ten3^{Het}$ and $Ten3^{KO}$. $^{****}P < 0.0001$ ($Ten3^{Het}$: $n = 12$; $Ten3^{KO}$: $n = 16$; two-tailed *t*-test). **h**, Diagram of stimulating electrode and recording sites. **i**, EPSC traces from proximal and distal subicular cells in $Ten3^{WT}$ and $Ten3^{KO}$ mice. **j**, Average EPSC amplitude in proximal (left) and distal (right) subicular cells from $Ten3^{WT}$ and $Ten3^{KO}$ mice at increasing stimulation intensities. Proximal: $Ten3^{WT}$, $n = 12$ cells; $Ten3^{KO}$, $n = 11$ cells; $P > 0.05$ for all stimulation intensities. Distal: $Ten3^{WT}$, $n = 14$ cells, 6 mice; $Ten3^{KO}$, $n = 9$ cells, 7 mice; 75 μA stimulation, $P = 0.035$; 100 μA stimulation, $P = 0.022$, adjusted *P* values from two-tailed *t*-tests with Holm–Šídák's correction. **k**, Paired pulse ratio for proximal (left) and distal (right) subicular cells from $Ten3^{WT}$ and $Ten3^{KO}$ mice. (Proximal: $Ten3^{WT}$, $n = 9$ cells, 6 mice; $Ten3^{KO}$, $n = 8$ cells, 7 mice; $P = 0.5566$. Distal, $Ten3^{WT}$: $n = 11$ cells, 6 mice; $Ten3^{KO}$: $n = 7$ cells, 7 mice; $P = 0.0049$, two-tailed *t*-test.) Scale bars, 200 μm. Error bars, mean ± s.e.m.

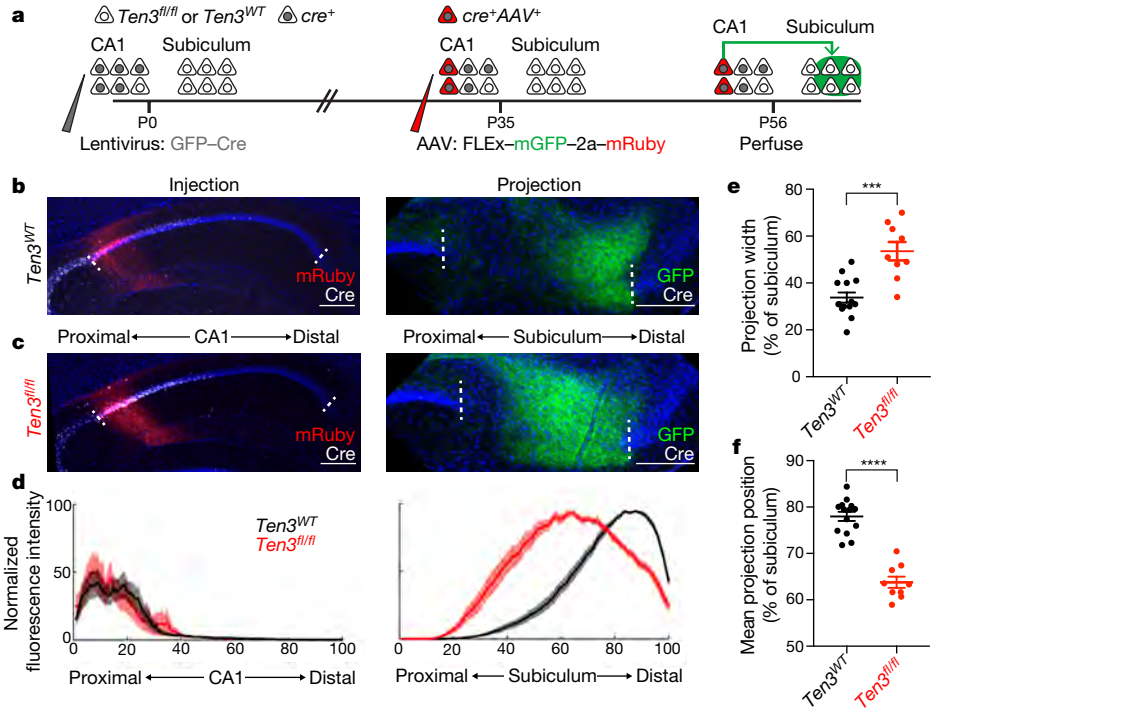


**Figure 3 | *Ten3* conditional knockout in CA1. a**, Experimental scheme. **b**, **c**, Adeno-associated virus (AAV) injections in proximal CA1 (left) and corresponding projections in subiculum (right) of $Ten3^{WT}$ (**b**) and $Ten3^{fl/fl}$ (**c**) mice. Red, injections; green, projections; white, Cre staining. **d**, Average normalized fluorescence intensity traces for proximal CA1 injections (left) and corresponding subicular projections (right) for control (black, $n = 14$) and CA1 conditional knockout (red, $n = 9$) mice. **e**, **f**, Projection width-at-half-maximum (**e**) and mean position (**f**) for control and knockout mice. $^{***}P = 0.0001$, $^{****}P < 0.0001$, two-tailed *t*-tests. Scale bars, 200 μm. Error bars, mean ± s.e.m.

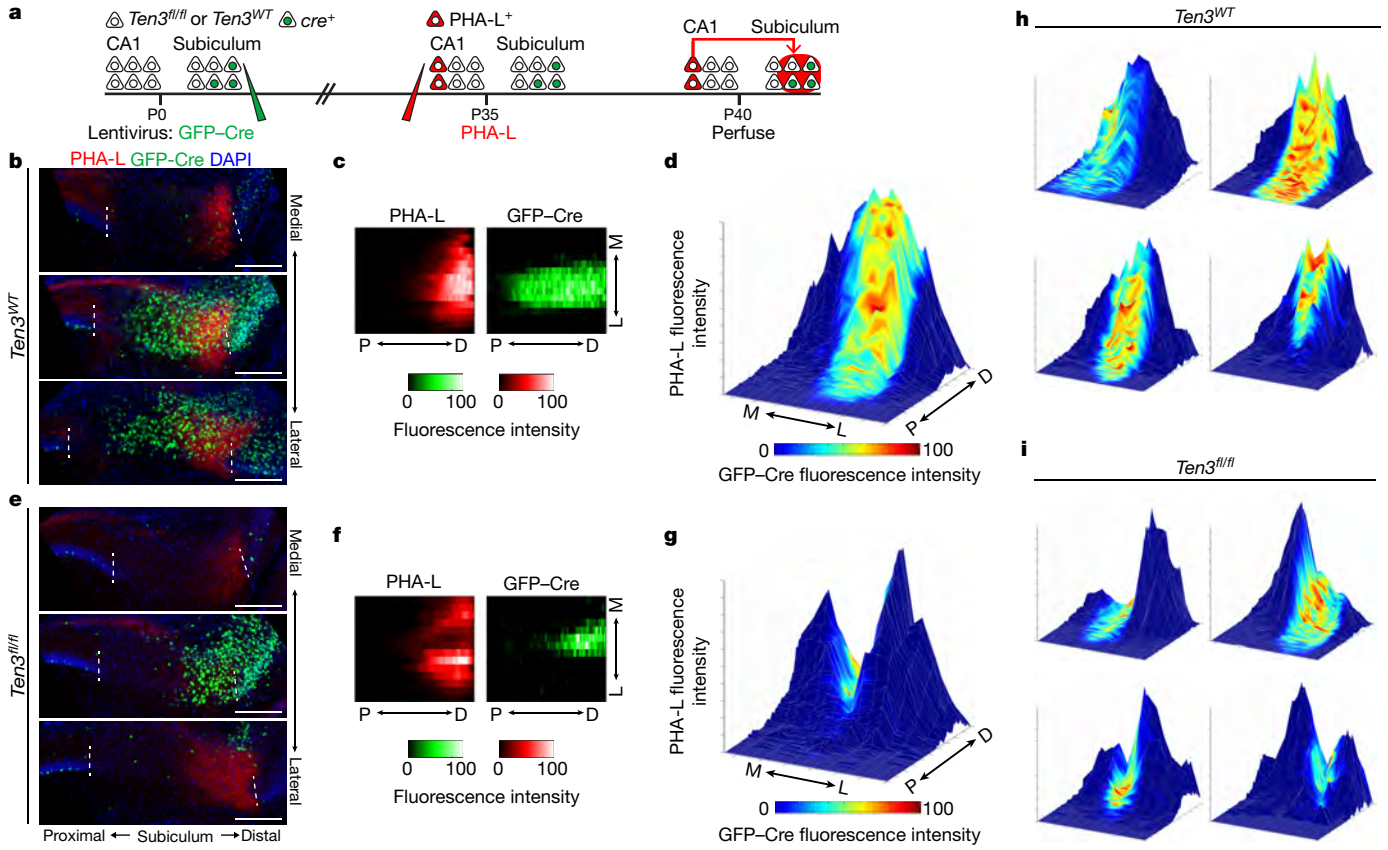


**Figure 4 | *Ten3* conditional knockout in subiculum. a**, Experimental scheme. **b**, **e**, Example images from $Ten3^{WT}$ (**b**) and $Ten3^{fl/fl}$ (**e**) mice, showing axons from proximal CA1 PHA-L injection in red, and GFP–Cre in subiculum in green. Three 60-μm sections are arranged from medial to lateral, 480–600 μm between sections. Scale bars, 200 μm. **c**, **f**, Heatmaps showing normalized PHA-L fluorescence intensity (red, left) and normalized GFP–Cre intensity (green, right) in subiculum, same mice as **b** and **e**. Each row is one section, 120 μm between rows. **d**, **g**, Surface plots showing normalized PHA-L intensity as height, and normalized GFP–Cre intensity as colour, same data as **b**, **c** and **e**, **f**, respectively. **h**, **i**, Surface plots from additional $Ten3^{WT}$ (**h**) and $Ten3^{fl/fl}$ (**i**) mice. See Extended Data Fig. 8 for all mice analysed.

neurons sent axons to distal subiculum as expected (Fig. 3b, d). In $Ten3^{fl/fl}$ mice, however, proximal CA1 axons covered most of subiculum, with their intensity peaking near the centre (Fig. 3c, d). The width of the projection was significantly increased in $Ten3^{fl/fl}$, and the mean position shifted proximally (Fig. 3d–f). Thus, Ten3 is required in CA1 neurons for their precise axon targeting in subiculum.

## Subiculum conditional knockout analysis

To test whether Ten3 is also required in subicular cells for CA1 axon targeting, we injected *cre*-expressing lentivirus into subiculum at P0, the anterograde tracer PHA-L into proximal CA1 at P35, and analysed the position of CA1 axons in subiculum (Fig. 4a). Because Cre expression covered a small region of subiculum relative to the target field of labelled CA1 axons, we asked whether CA1 axons targeted differently within Cre-expressing regions versus nearby Cre-negative regions. In $Ten3^{WT}$ controls, CA1 axons were unaffected when projecting into Cre-expressing subicular areas, as analysed in serial histological sections (Fig. 4b, c and Extended Data Fig. 8a, c). In $Ten3^{fl/fl}$ mice, however, labelled CA1 axons appeared to avoid the patch of Cre-expressing, *Ten3*-deleted subicular cells (Fig. 4e, f and Extended Data Fig. 8b, d).

To visualize the relationship between the CA1→subiculum axon projections and GFP–Cre expression in the target, we plotted the intensities of CA1 axons and GFP–Cre on the same graph as height and colour, respectively. While Cre expression ('hot' coloured) did not affect the projection strength (height) in $Ten3^{WT}$ controls (Fig. 4d, h and Extended Data Fig. 8c), the projection strength was severely diminished in Cre-expressing patches in $Ten3^{fl/fl}$ mice (Fig. 4g, i and Extended Data Fig. 8d). Because we only made a focal deletion of *Ten3* in subiculum with the lentivirus injection, there were many Ten3-expressing cells in nearby regions of distal subiculum. The simplest interpretation for this drastic phenotype is that Ten3-high proximal CA1 axons destined for the Ten3-deleted patch mistargeted to nearby Ten3-high distal regions, consistent with Ten3 in distal subiculum acting as an attractant for proximal CA1 axons (Fig. 5f).

## Ten3 promotes homophilic adhesion

If Ten3 functions as a homophilic cell adhesion molecule as previously proposed[28,29,43], it could directly mediate the recognition of Ten3-expressing target cells by Ten3-expressing axons. Ten3 has alternatively spliced isoforms that differ by the inclusion or exclusion of exon 12 and exon 20 (at splice sites A and B, hereafter) encoding 9- and 7-amino-acid peptides in the extracellular epidermal growth factor-like (EGF-like) and NCL-1, HT2A, and Lin-41 (NHL) repeats, respectively[44,45] (Fig. 5a, b). We denote the splicing at site A as $A_0$ (exon 12 excluded) or $A_1$ (exon 12 included), and at site B as $B_0$ (exon 20 excluded) or $B_1$ (exon 20 included). We sequenced *Ten3* cDNA clones from CA1 or subiculum at P8, a time when the CA1→subiculum projection was still developing (Extended Data Fig. 7). We found two additional alternative splicing variants at site A (termed $A_2$ and $A_3$) that were computationally predicted[46]; the inclusion of these exons (12.1 or 12.2) would add six or seven additional amino acids to exon-12-containing variants (Fig. 5a, b). Overall, CA1 and subiculum expressed similar splicing isoforms, most of which included inserts at sites A and B (Fig. 5c).

We next performed cell aggregation experiments, and found that all isoforms tested promoted homophilic adhesion except $A_0B_0$, which

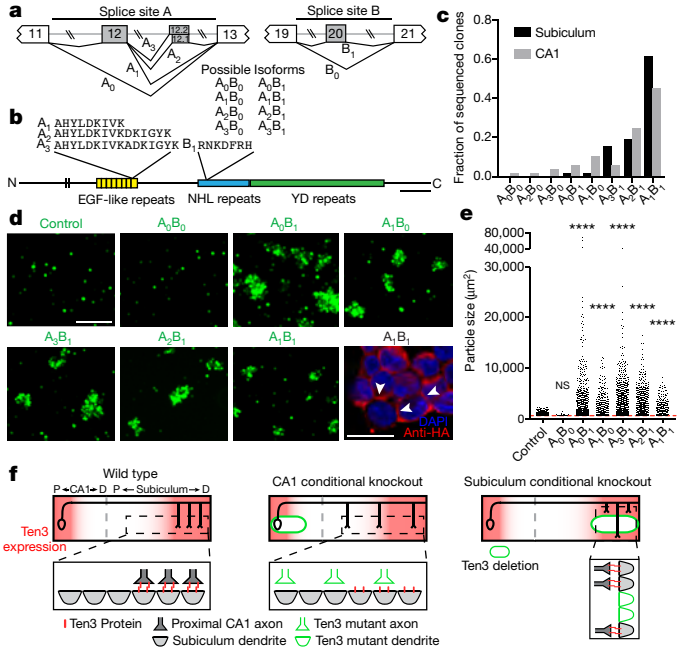


**Figure 5 | Ten3 promotes homophilic adhesion in a splicing isoform-dependent manner. a**, Partial *Ten3* genomic regions (top) highlighting alternatively spliced exons (grey boxes) and constitutive exons (white boxes). Splice variant names are next to corresponding splicing pattern. **b**, Locations of alternative splicing sites A and B in Ten3 protein, and amino acid sequences produced. YD, tyrosine and aspartate. Scale bar, 200 amino acids. **c**, Summary of cDNA sequencing from P8 subiculum ($n = 52$ clones) and CA1 ($n = 49$ clones). **d**, Aggregation of K562 cells expressing different Ten3 isoforms and GFP. Scale bar, 200 μm. Bottom right: $A_1B_1$ aggregate stained for the N-terminal haemagglutinin (HA) tag (red). Arrowheads highlight membrane-localized Ten3 at cell–cell junctions. Scale bar, 20 μm. **e**, Quantification of aggregate sizes pooled from three biological replicates. Dotted red line shows size cutoff at 600 $\mu m^2$. NS, not significant; $^{****}P \leq 0.0001$, adjusted *P* values from Dunn's multiple comparisons test after Kruskal–Wallis test, comparing all conditions to GFP. GFP, $n = 1449$ particles above threshold; $A_0B_0$, $n = 26$; $A_0B_1$, $n = 1179$; $A_1B_0$, $n = 411$; $A_3B_1$, $n = 1268$; $A_2B_1$, $n = 628$; $A_1B_1$, $n = 336$. **f**, Summary of data (top) and working model (bottom). KO, knockout. See Discussion for details.

lacks all alternatively spliced exons (Fig. 5d, e). $A_0B_0$ was functionally expressed because it promoted adhesion with latrophilin-3-expressing cells (Extended Data Fig. 9), as previously reported for other teneurin and latrophilin family proteins[30]. The $A_0B_0$ isoform occurred in only one out of 101 sequenced clones, indicating that most Ten3 isoforms present in CA1 and subiculum were capable of interacting in *trans* to promote homophilic adhesion. When the three highest-expressed isoforms of Ten3 were tested in a mixed cell aggregation assay, all aggregates were mixed, indicating that the major Ten3 isoforms expressed in the hippocampus can interact with each other in *trans* (Extended Data Fig. 10). Together with the matching expression and conditional knockout phenotypes, these data suggest that homophilic Ten3 interactions between CA1 axons and subicular cell bodies and dendrites control the targeting specificity of proximal CA1 axons to distal subiculum.

## Discussion

A striking feature of neural development is the formation of highly precise connections between neurons. Sensory and motor circuits have been extensively used to characterize the molecular control of wiring specificity[11,12,47,48], but relatively little is known about how neurons in complex high-order circuits find appropriate partners. Here, we have shown that Ten3 acts in both pre- and postsynaptic neurons in the hippocampus to control the assembly of a precise topographic projection. Loss-of-function phenotypes support a homophilic attraction mechanism: when Ten3 is lost from CA1 neurons, proximal CA1 axons spread throughout the entire subiculum, instead of projecting only to distal, Ten3-high targets; when Ten3 is lost from a subset of distal subicular cells, Ten3-high proximal CA1 axons do not target these areas and instead innervate nearby Ten3-high regions (Fig. 5f). Our *in vitro* data further show that Ten3 can interact homophilically in *trans*, supporting a model in which Ten3 on CA1 axons interacts with Ten3 on subicular targets, leading to contact-mediated attraction or stabilization of proximal CA1 axons by distal subicular target cells. This mechanism of action resembles that of the *Drosophila* teneurins in the development of olfactory and neuromuscular connections, suggesting an evolutionarily conserved mode of teneurin function in neural circuit assembly from insects to mammals. However, whereas *Drosophila* teneurins instruct matching of discrete types of pre- and postsynaptic cell, the graded expression in both CA1 and subiculum suggests that mouse Ten3 directs continuous topographic mapping along the proximal–distal axis (Fig. 5f).

Our model does not exclude the possibility that interactions of Ten3 with heterophilic partners have additional roles in circuit assembly. While in many cases we observed Ten3 expression in both pre- and postsynaptic partners of specific connections, there were also cases where Ten3 was only observed in axons but not targets (for example, MEC→dentate gyrus–CA3). Further, the $A_0B_0$ isoform did not exhibit homophilic interactions but did interact heterophilically with latrophilin-3. These observations suggest that interactions between Ten3 and latrophilins or other potential heterophilic partners may also contribute to wiring specificity.

Our results highlight small regions of Ten3 that are critical for *trans* interactions. Splice site A corresponds to the most C-terminal of the eight EGF-like repeats, which are thought to mediate *cis*-dimerization of teneurin proteins[44,49]. Our results suggest that the EGF-like repeats may also participate in *trans* interactions, or that teneurin *cis* interactions may influence *trans* interactions. Splice site B is within the NHL-repeat region, which was implicated in homophilic teneurin interactions using single-cell force spectroscopy[29]. Our result supports the importance of the NHL repeats, and identifies specific residues that are required for homophilic interactions.

What controls the distal CA1→proximal subiculum projection? Since none of the other three mouse teneurins exhibited differential expression along the proximal–distal axis of the hippocampal formation[16], other differentially expressed proteins might act in parallel with Ten3 to control the distal CA1→proximal subiculum projection. Axon–axon competition could also contribute, as in retinotopic map development[50]. Indeed, the enhanced severity of the CA1-specific conditional knockout phenotype compared with the whole-animal $Ten3^{KO}$ phenotype (Fig. 3d–f versus Fig. 2e–g) may result from Ten3-expressing CA1 axons out-competing mutant axons for space in distal subiculum, supporting a role of axon–axon competition in determining CA1→subiculum targeting specificity.

Finally, our findings reveal genetic heterogeneity within many areas of the hippocampal region. Although our genetic analyses focused on the CA1→subiculum projection, Ten3-high to Ten3-high connectivity was also observed in the entorhinal→hippocampal projections (Fig. 1d–f), and probably exists in additional hippocampus-associated projections (Extended Data Fig. 3). The matching expression of Ten3 in multiple topographically connected subregions, combined with our loss-of-function and *in vitro* data, suggests that Ten3 may control the assembly of a widely distributed circuit in mammalian brains.

**Online Content** Methods, along with any additional Extended Data display items and Source Data, are available in the online version of the paper; references unique to these sections appear only in the online paper.

**Received 17 June; accepted 19 December 2017.**
**Published online 7 February 2018.**

1. Scoville, W. B. & Milner, B. Loss of recent memory after bilateral hippocampal lesions. *J. Neurol. Neurosurg. Psychiatry* **20,** 11–21 (1957).
2. Squire, L. R., Stark, C. E. L. & Clark, R. E. The medial temporal lobe. *Annu. Rev. Neurosci.* **27,** 279–306 (2004).
3. O'Keefe, J. & Dostrovsky, J. The hippocampus as a spatial map. Preliminary evidence from unit activity in the freely-moving rat. *Brain Res.* **34,** 171–175 (1971).
4. Hafting, T., Fyhn, M., Molden, S., Moser, M. B. & Moser, E. I. Microstructure of a spatial map in the entorhinal cortex. *Nature* **436,** 801–806 (2005).
5. van Strien, N. M., Cappaert, N. L. M. & Witter, M. P. The anatomy of memory: an interactive overview of the parahippocampal–hippocampal network. *Nat. Rev. Neurosci.* **10,** 272–282 (2009).
6. Tamamaki, N. & Nojyo, Y. Preservation of topography in the connections between the subiculum, field CA1, and the entorhinal cortex in rats. *J. Comp. Neurol.* **353,** 379–390 (1995).
7. Naber, P. A., Lopes da Silva, F. H. & Witter, M. P. Reciprocal connections between the entorhinal cortex and hippocampal fields CA1 and the subiculum are in register with the projections from CA1 to the subiculum. *Hippocampus* **11,** 99–104 (2001).
8. Igarashi, K. M., Ito, H. T., Moser, E. I. & Moser, M. B. Functional diversity along the transverse axis of hippocampal area CA1. *FEBS Lett.* **588,** 2470–2476 (2014).
9. Cembrowski, M. S. *et al.* Spatial gene-expression gradients underlie prominent heterogeneity of CA1 pyramidal neurons. *Neuron* **89,** 351–368 (2016).
10. Sperry, R. W. Chemoaffinity in the orderly growth of nerve fiber patterns and connections. *Proc. Natl Acad. Sci. USA* **50,** 703–710 (1963).
11. Sanes, J. R. & Yamagata, M. Many paths to synaptic specificity. *Annu. Rev. Cell Dev. Biol.* **25,** 161–195 (2009).
12. Kolodkin, A. L. & Tessier-Lavigne, M. Mechanisms and molecules of neuronal wiring: a primer. *Cold Spring Harb. Perspect. Biol.* **3,** 1–14 (2011).
13. Hong, W., Mosca, T. J. & Luo, L. Teneurins instruct synaptic partner matching in an olfactory map. *Nature* **484,** 201–207 (2012).
14. Mosca, T. J., Hong, W., Dani, V. S., Favaloro, V. & Luo, L. Trans-synaptic Teneurin signalling in neuromuscular synapse organization and target choice. *Nature* **484,** 237–241 (2012).
15. Tucker, R. P., Beckmann, J., Leachman, N. T., Schöler, J. & Chiquet-Ehrismann, R. Phylogenetic analysis of the teneurins: conserved features and premetazoan ancestry. *Mol. Biol. Evol.* **29,** 1019–1029 (2012).
16. Li, H., Bishop, K. M. & O'Leary, D. D. M. Potential target genes of EMX2 include *odz/Ten-m* and other gene families with implications for cortical patterning. *Mol. Cell. Neurosci.* **33,** 136–149 (2006).
17. Psychiatric GWAS Consortium Bipolar Disorder Working Group. Large-scale genome-wide association analysis of bipolar disorder identifies a new susceptibility locus near *ODZ4*. *Nat. Genet.* **43,** 977–983 (2011).
18. Green, E. K. *et al.* Replication of bipolar disorder susceptibility alleles and identification of two novel genome-wide significant associations in a new bipolar disorder case-control sample. *Mol. Psychiatry* **18,** 1302–1307 (2013).
19. Mühleisen, T. W. *et al.* Genome-wide association study reveals two new risk loci for bipolar disorder. *Nat. Commun.* **5,** 3339 (2014).
20. Croarkin, P. E. *et al.* Genetic risk score analysis in early-onset bipolar disorder. *J. Clin. Psychiatry* **78,** 1337–1343 (2017).
21. Ivorra, J. L. *et al.* Replication of previous genome-wide association studies of psychiatric diseases in a large schizophrenia case-control sample from Spain. *Schizophr. Res.* **159,** 107–113 (2014).
22. Aldahmesh, M. A., Mohammed, J. Y., Al-Hazzaa, S. & Alkuraya, F. S. Homozygous null mutation in *ODZ3* causes microphthalmia in humans. *Genet. Med.* **14,** 900–904 (2012).
23. Alkelai, A. *et al.* A role for *TENM1* mutations in congenital general anosmia. *Clin. Genet.* **90,** 211–219 (2016).
24. Leamey, C. A. *et al.* Ten_m3 regulates eye-specific patterning in the mammalian visual pathway and is required for binocular vision. *PLoS Biol.* **5,** e241 (2007).
25. Dharmaratne, N. *et al.* Ten-m3 is required for the development of topography in the ipsilateral retinocollicular pathway. *PLoS ONE* **7,** e43083 (2012).
26. Antinucci, P., Nikolaou, N., Meyer, M. P. & Hindges, R. Teneurin-3 specifies morphological and functional connectivity of retinal ganglion cells in the vertebrate visual system. *Cell Reports* **5,** 582–592 (2013).
27. Antinucci, P., Suleyman, O., Monfries, C. & Hindges, R. Neural mechanisms generating orientation selectivity in the retina. *Curr. Biol.* **26,** 1802–1815 (2016).
28. Rubin, B. P., Tucker, R. P., Brown-Luedi, M., Martin, D. & Chiquet-Ehrismann, R. Teneurin 2 is expressed by the neurons of the thalamofugal visual system in situ and promotes homophilic cell-cell adhesion in vitro. *Development* **129,** 4697–4705 (2002).
29. Beckmann, J., Schubert, R., Chiquet-Ehrismann, R. & Müller, D. J. Deciphering teneurin domains that facilitate cellular recognition, cell-cell adhesion, and neurite outgrowth using atomic force microscopy-based single-cell force spectroscopy. *Nano Lett.* **13,** 2937–2946 (2013).
30. Boucard, A. A., Maxeiner, S. & Südhof, T. C. Latrophilins function as heterophilic cell-adhesion molecules by binding to teneurins: regulation by alternative splicing. *J. Biol. Chem.* **289,** 387–402 (2014).
31. Silva, J.-P. *et al.* Latrophilin 1 and its endogenous ligand Lasso/teneurin-2 form a high-affinity transsynaptic receptor pair with signaling capabilities. *Proc. Natl Acad. Sci. USA* **108,** 12113–12118 (2011).
32. O'Sullivan, M. L. *et al.* FLRT proteins are endogenous latrophilin ligands and regulate excitatory synapse development. *Neuron* **73,** 903–910 (2012).
33. Loh, K. H. *et al.* Proteomic analysis of unbounded cellular compartments: synaptic clefts. *Cell* **166,** 1295–1307 (2016).
34. Steward, O. Topographic organization of the projections from the entorhinal area to the hippocampal formation of the rat. *J. Comp. Neurol.* **167,** 285–314 (1976).
35. van Groen, T., Miettinen, P. & Kadish, I. The entorhinal cortex of the mouse: organization of the projection to the hippocampal formation. *Hippocampus* **13,** 133–149 (2003).
36. Muraoka, D., Katsuyama, Y., Kikkawa, S. & Terashima, T. Postnatal development of entorhinodentate projection of the Reeler mutant mouse. *Dev. Neurosci.* **29,** 59–72 (2007).
37. Tamamaki, N. & Nojyo, Y. Disposition of the slab-like modules formed by axon branches originating from single CA1 pyramidal neurons in the rat hippocampus. *J. Comp. Neurol.* **291,** 509–519 (1990).
38. Amaral, D. G., Dolorfo, C. & Alvarez-Royo, P. Organization of CA1 projections to the subiculum: a PHA-L analysis in the rat. *Hippocampus* **1,** 415–435 (1991).
39. Honda, Y. & Ishizuka, N. Topographic distribution of cortical projection cells in the rat subiculum. *Neurosci. Res.* **92,** 1–20 (2015).
40. Witter, M. P. & Groenewegen, H. J. The subiculum: cytoarchitectonically a simple structure, but hodologically complex. *Prog. Brain Res.* **83,** 47–58 (1990).
41. Gerfen, C. R. & Sawchenko, P. E. An anterograde neuroanatomical tracing method that shows the detailed morphology of neurons, their axons and terminals: immunohistochemical localization of an axonally transported plant lectin, *Phaseolus vulgaris* leucoagglutinin (PHA-L). *Brain Res.* **290,** 219–238 (1984).
42. Mosca, T. J. & Luo, L. Synaptic organization of the *Drosophila* antennal lobe and its regulation by the Teneurins. *eLife* **3,** e03726 (2014).
43. Leamey, C. A. *et al.* Differential gene expression between sensory neocortical areas: potential roles for Ten_m3 and Bcl6 in patterning visual and somatosensory pathways. *Cereb. Cortex* **18,** 53–66 (2008).
44. Oohashi, T. *et al.* Mouse Ten-m/Odz is a new family of dimeric type II transmembrane proteins expressed in many tissues. *J. Cell Biol.* **145,** 563–577 (1999).
45. Ben-Zur, T., Feige, E., Motro, B. & Wides, R. The mammalian Odz gene family: homologs of a *Drosophila* pair-rule gene with expression implying distinct yet overlapping developmental roles. *Dev. Biol.* **217,** 107–120 (2000).
46. O'Leary, N. A. *et al.* Reference sequence (RefSeq) database at NCBI: current status, taxonomic expansion, and functional annotation. *Nucleic Acids Res.* **44** (D1), D733–D745 (2016).
47. Luo, L. & Flanagan, J. G. Development of continuous and discrete neural maps. *Neuron* **56,** 284–300 (2007).
48. Bonanomi, D. & Pfaff, S. L. Motor axon pathfinding. *Cold Spring Harb. Perspect. Biol.* **2,** a001735 (2010).
49. Feng, K. *et al.* All four members of the Ten-m/Odz family of transmembrane proteins form dimers. *J. Biol. Chem.* **277,** 26128–26135 (2002).
50. Triplett, J. W. *et al.* Competition is a driving force in topographic mapping. *Proc. Natl Acad. Sci. USA* **108,** 19060–19065 (2011).


**Supplementary Information** is available in the online version of the paper.

**Acknowledgements** We thank C. Guo and the Howard Hughes Medical Institute/Janelia Research Campus for producing the *Ten3*$^{cre}$ and *Ten3*$^{fl}$ alleles, M. Sur for providing the *Ten3*$^{\Delta 4}$ allele, the Neuroscience Gene Vector and Virus Core at Stanford for producing viruses, K. DeLoach for technical assistance, T. Mosca and W. Hong for advice and inspiration, members of the Luo laboratory for discussion and support, P. Thomas for the dual transcription unit vector, T. Südhof for advice and the latrophilin-3 construct, and K. Shen, L. Giocomo, T. Mosca, H. Li, J. Li, J. Lui, E. Richman and A. Shuster for critiques of the manuscript. D.S.B. was supported by a National Institute on Deafness and Other Communication Disorders predoctoral fellowship (F31DC013240), L.A.D. was supported by an National Institute of Neurological Disorders and Stroke postdoctoral fellowship (F32NS087860) and L.L. is an investigator of Howard Hughes Medical Institute. This work was supported by a National Institutes of Health grant (R01-NS050580 to L.L.).

**Author Contributions** D.S.B. performed all the experiments and analysed the data except the electrophysiology experiments. L.A.D. performed the electrophysiology experiments and analysed the data. D.T.P. assisted in aggregation assays. L.L. supervised the project. D.S.B. and L.L. wrote the paper.

**Author Information** Reprints and permissions information is available at www.nature.com/reprints. The authors declare no competing financial interests. Readers are welcome to comment on the online version of the paper. Publisher's note: Springer Nature remains neutral with regard to jurisdictional claims in published maps and institutional affiliations. Correspondence and requests for materials should be addressed to L.L. (lluo@stanford.edu).

**Reviewer Information** *Nature* thanks M. Witter and the other anonymous reviewer(s) for their contribution to the peer review of this work.

## METHODS

**Statistics and reproducibility.** All statistical analyses were performed in Prism 7 (GraphPad). No statistical methods were used to determine sample size. The experiments were not randomized. Experimenters were blind to genotype during injections and analysis of axon tracing, but not for electrophysiology or other experiments. Images of Ten3 immunostaining and *in situ* hybridization (Figs 1a, b and 2a and Extended Data Figs 1b–j, 3a–g, 4b–d and 6b–d) are representative of at least three separate experiments in all cases. Images of entorhinal cortex axon tracing (Fig. 1d, e) are representative of three injections. For developmental tracing, images shown are representative of three (P2 and P4) or two (P6 and P8) experiments. For subiculum conditional knockout (Fig. 4 and Extended Data Fig. 8), results from all experiments are shown in Extended Data Fig. 8.

**Mice.** All animal procedures followed animal care guidelines approved by Stanford University's Administrative Panel on Laboratory Animal Care. Both male and female mice were used, and mice were group housed. CD-1 mice from Charles River Laboratories were used for all wild-type expression studies. *Ten3*$^{\Delta 4}$ mice[24] were provided by M. Sur and maintained on a CD-1 background. *Ten3*$^{cre}$ and *Ten3*$^{fl}$ were maintained on mixed CD-1, C57BL/6, and 129 backgrounds. *Ten3*$^{cre}$ mice used in this study still had the neomycin resistance cassette (Neo) in the genome. *Ten3*$^{fl}$ mice were crossed to a germline-active GFP–FlpO line[51] to delete the Neo. Both Neo-deleted and Neo-containing *Ten3*$^{fl}$ mice were used for Figs 3 and 4.

**Generation of *Ten3*$^{cre}$ and *Ten3*$^{fl}$ mice.** Mice were generated by the Gene Targeting and Transgenics core at Janelia Research Campus. *Ten3*$^{cre}$ was generated by homologous recombination in embryonic stem cells using standard procedures. *Ten3*$^{fl}$ was generated by co-injection of the targeting construct with *Cas9* mRNA and guide RNAs targeted just outside the *loxP* sites. Target sequences for gRNAs were GGGTGTCTAGAAAGTCAGTG AGG and AAAGTCCTTCATGGGCT TGC AGG. Targeting was verified in embryonic stem cells by long-arm PCR. After microinjection, chimaeras were bred with CD-1 females and $F_1$ offspring were screened by long-arm PCR and Southern blot to identify mice with germline transmission of the correctly targeted construct.

**Generation and affinity purification of Ten3 antibodies.** Rabbit polyclonal antibodies (produced by YenZym Antibodies) were raised to the following peptides: Ten3IC (used in main figures), amino acids 163–176 (C)ENRSDSESEQPSNN; Ten3EC, amino acids 346–364 (C)DTFENGKVNSDTVPTNTVS. Affinity purification from serum was performed using target peptides immobilized on SulfoLink columns (Thermo Fisher, 44999). Peptides were coupled to columns following the manufacturer's instructions. After blocking and washing, 2 ml antiserum mixed with 2 ml PBS, pH 7.4, was added to the column, and left on a nutator overnight at 4 °C. The next day, columns were washed with 40 ml PBS pH 7.4, 40 ml PBS pH 7.4 + 0.5 M NaCl, and 40 ml PBS pH 7.4, all by gravity flow. Columns were eluted with 20 ml 100 mM glycine pH 2.5. Fractions (1 ml) were collected into tubes containing 60 µl 1 M Tris-HCl pH 8.8 for neutralization. All washes and elutions were performed at room temperature. Antibody concentration was measured using $A_{280\,nm}$ on a NanoDrop 1000, immunoglobulin-G setting. Fractions containing protein were combined and dialysed against PBS, pH 7.4, using Slide-a-lyzer cassettes (Thermo Fisher, 66380). Antibody concentration was measured again using $A_{280\,nm}$, and BSA (Thermo Fisher, 15561020) was added to raise total protein concentration to 1 mg ml$^{-1}$. Aliquots were snap frozen in liquid nitrogen and stored at −80 °C.

**Immunostaining.** Mice were given an overdose of 2.5% Avertin and were perfused transcardially with PBS followed by 4% paraformaldehyde (by weight) in PBS. For Ten3 immunostaining, brains were dissected, post-fixed in 4% paraformaldehyde for 1 h, and cryoprotected for 24–48 h in 30% sucrose. For all other immunostaining, brains were dissected, post-fixed in 4% paraformaldehyde for 12–24 h, and placed in 30% sucrose for 24–48 h. They were then embedded in Optimum Cutting Temperature (OCT, Tissue-Tek) on dry ice and stored at −80 °C until sectioning. Floating sections (60 µm) were collected into PBS. Sections were incubated in the following solutions at room temperature unless otherwise indicated: 1 × 5–10 min in PBS, 1 h in 0.3% PBS/Triton X-100 (PBST) and 10% normal donkey serum (NDS), two to four nights in primary antibody at 4 °C in 5% NDS in PBST, 2 × 15 min in PBST, 2 h in secondary antibody in 5% NDS in PBST, 2 × 15 min in PBST, 30 min in DAPI (1:10,000 of 5 mg ml$^{-1}$, Sigma-Aldrich) in PBS, and 5–10 min in PBS. Sections were mounted on Superfrost Plus slides and coverslipped with Fluoromount-G (SouthernBiotech). For adult Ten3 staining, tissue was fixed overnight. Antigen retrieval on sections was performed in 10 mM sodium citrate, pH 8.5, at 80 °C for 30 min. Tissue was allowed to cool, washed three times with PBS, then blocked and immunostained as above. Primary antibodies used were rabbit anti-Ten3IC (1:1,000, four nights in primary antibody); rabbit anti-Ten3EC (1:200, four nights in primary antibody), mouse anti-Cre (1:1,000, Millipore, MAB3120), rabbit anti-PHA-L (1:1,000, Vector Labs, AS-2300, two nights in primary), chicken anti-GFP (1:2,500, Aves Labs, GFP-1020), and rat anti-mCherry (1:1,000, Thermo Fisher, M11217). Secondary antibodies conjugated to Alexa 488, Alexa 647, or Cy3 (Jackson ImmunoResearch) were used at 1:500 from 50% glycerol stocks. For Biotinylated Dextran Amine (BDA) axon tracing, sections were washed for 5 min in PBS, incubated in PBST for 30 min, 1:200 streptavidin-Cy3 in PBST overnight, washed 3 × 15 min in PBST, and stained with DAPI and mounted as described above. Sections were imaged on Zeiss epifluorescence and 780 confocal microscopes and on a Leica Ariol automated fluorescence slide scanning system. Images were processed in FIJI to stitch multiple fields-of-view of single sections and to adjust contrast and brightness of each channel. Images presented together were processed identically.

***In situ* hybridization.** *In situ* hybridization was performed as previously described[52] with the following modifications. Cryosections (12–16 µm) were collected on Superfrost Plus slides. *Ten3* probe containing base pairs 4124–4953 of *Ten3* mRNA (located in exon 23; mRNA accession number NM_011857.3) was PCR amplified from genomic DNA using the following primers: 5′-GTGGCTAAAAGCCCACTGTTGCC-3′, 5′-GAATGGCC CACTGACCTCGCG-3′. PCR product was cloned into pCR4-TOPO (K457502). RNA probes were transcribed using T3 or T7 RNA polymerases. For colorimetric development (Fig. 1d), Sigma-FAST NBT/BCIP (Sigma, B5655) was used. For combined *in situ* hybridization with immunostaining (Extended Data Fig. 1j) hybridized slides were incubated overnight with alkaline phosphatase-conjugated anti-DIG antibody (1:1,000, Roche Applied Science, 1093274) and rabbit anti-PCP4 (1:200, Sigma, HPA005792). Signals were developed using Fast Red TR/Naphthol As-MX (Sigma-Aldrich, F4523) and 488 donkey anti-rabbit secondary (1:200, Jackson Immunoresearch). Sections were imaged on Zeiss epifluorescence and 780 confocal microscopes. For fluorescent *in situ* hybridization for quantification, 12 µm sections of P10 brain were used. Sagittal sections were taken from dorsal hippocampus, and horizontal sections were from middle levels of the dorsal–ventral axis. After hybridization, washing, and blocking, slides were incubated with alkaline phosphatase-conjugated anti-DIG antibody (1:1,000) for 1 h and developed with Fast Red TR/Naphthol As-MX for 45 min. Sections were imaged at 10× magnification on a Zeiss epifluorescence scope. Fluorescence intensity measurements were taken on unprocessed images in FIJI and data were processed using custom MATLAB scripts. For CA1 quantifications, a 45-pixel-wide segmented line with spline fit was drawn along CA1, from proximal to distal. Intensity values along the CA1 line were measured using the Plot Profile command. For quantification of subiculum, a 125-pixel-wide segmented line with spline fit was drawn along subiculum, from proximal to distal. The bottom of the line was aligned to the superficial border of the subicular pyramidal cell layer; the proximal border of subiculum was defined in the same way as the distal border of CA1: that is, the point where the compact CA1 cell body layer ended. The distal subiculum border was defined by the increase in cell density of presubiculum layer 2. Because of the narrowing of the distal subicular cell layer, the line was drawn until the *Ten3* fluorescent signal became narrower than the 125-pixel line, to avoid averaging areas with zero signal. This resulted in the exclusion of a small portion of the *Ten3* signal in the most distal subiculum. Identical background subtraction was performed on all intensity traces, on the basis of the signal in sense control slides. The intensity traces were binned into 100 bins from proximal to distal, and the traces for individual sections were normalized to a peak of 100. Traces for individual sections were then averaged to produce intensity plots. Numbers of sections were as follows: sagittal and horizontal CA1, 12 sections, 4 mice; sagittal and horizontal subiculum, 14 sections, 4 mice.

**Electrophysiology.** At P14–P19, the brain was removed and placed in ice-cold carbogenated slicing artificial cerebrospinal fluid that contained (in mM) 83 NaCl, 2.5 KCl, 1 $NaH_2PO_4$, 26.2 $NaHCO_3$, 22 glucose, 72 sucrose, 0.5 $CaCl_2$, and 3.3 $MgSO_4$. Coronal sections (300 µm) were cut on a Leica vibratome. Slices were allowed to recover at 31 °C for 40 min and then at 23–25 °C for 30 min to 6 h. Slices were then placed in carbogenated recording artificial cerebrospinal fluid (119 NaCl, 2.5 KCl, 26 $NaHCO_3$, 1 $NaH_2PO_4$, 1.5 $MgSO_4$, 2.5 $CaCl_2$, and 11 glucose, all in mM) that contained 50 µM picrotoxin (Sigma). Signals were recorded with a 5× gain, low-pass filtered at 2 kHz, digitized at 10 kHz (Molecular Devices Multiclamp 700B), and analysed with pClamp 10 (Molecular Devices). Whole-cell recordings were made using 3–5 MΩ pipettes filled with an internal solution that contained (in mM) 123 caesium gluconate, 8 NaCl, 1 $CaCl_2$, 10 EGTA, 10 HEPES, and 10 glucose, pH 7.3, with CsOH, 280–290 mOsm. Series resistance ($R_s$) and input resistance ($R_{in}$) were monitored throughout the experiment by measuring the capacitive transient and steady-state deflection, respectively, in response to a −5 mV test pulse. $R_s$ and $R_{in}$ did not differ across experimental conditions (proximal subiculum recordings: $R_s$ wild type = 4.397 ± 0.157 MΩ, $n$ = 12; Ten3 knockout = 4.865 ± 0.417 MΩ, $n$ = 11; $P$ = 0.289, Student's $t$-test; $R_{in}$ in wild type = 201.6 ± 18.7 MΩ, $n$ = 12; Ten3 knockout = 253.1 ± 28.64 MΩ, $n$ = 11; $P$ = 0.141, Student's $t$-test; distal subiculum recordings: $R_s$ wild type = 4.409 ± 0.114 MΩ, $n$ = 14; Ten3

knockout = 4.561 ± 0.213 MΩ, $n = 9$; $P = 0.502$, Student's $t$-test; $R_{in}$ wild type = 221.8 ± 29.57 MΩ, $n = 14$; Ten3 knockout = 254.6 ± 34.83 MΩ, $n = 9$; $P = 0.486$, Student's $t$-test). Responses were evoked by a platinum two-contact cluster electrode (FHC) placed in the stratum oriens–alveus above distal CA1, at the stimulation intensities listed in the figure. Cells were clamped at −60 mV to measure GluA (AMPA-receptor)-mediated EPSC. Analysis was based on the average of ten sweeps. The inter-stimulus interval for paired pulse ratio measurements was 50 ms.

**Stereotactic surgery.** For stereotactic injections in neonatal mice, hypothermia was used for anaesthesia. Coordinates were zeroed from lambda. For CA1, coordinates used were 1 mm lateral, 1.1 mm anterior, 0.85 mm ventral from skull. For subiculum, coordinates were 1.1 mm lateral, 0.3 mm anterior, 0.8 ventral from skull. For developmental axon tracing, BDA (Thermo Fisher D1956, 5% in PBS) was iontophoretically injected into CA1 using a Digital Midgard Precision Current Source (Stoelting, 51595), pulled glass micropipettes (World Precision Instruments, 1B120F4) with tips broken to outer diameter of 10 μm, and current parameters 5 μA, alternating 7-s on, 7-s off, for 2 min. Mice were perfused between 2 and 8 days post-injection for histology as above. For conditional knockout experiments, 100 nl of lentivirus containing *Ub–GFP–cre* ($4.6 \times 10^8$ to $6.8 \times 10^8$ infectious units per microlitre, Neuroscience Gene Vector and Virus core, Stanford University) was injected at 100 nl min$^{-1}$. Subsequent injections of PHA-L or AAV8-hSyn1-FLEx–mGFP–2a-synaptophysin–mRuby[53] were performed at P35–P40. For whole-animal knockout studies, PHA-L was injected between P30 and P45. Mice were anaesthetized with ketamine-xylazine (Lloyd Laboratories) or isoflurane and immobilized in stereotactic apparatus (Kopf). Coordinates were proximal CA1 (from bregma) 1.4 mm lateral, 1.25–1.3 mm posterior, 1.1–1.2 mm ventral from brain surface; distal CA1 1.4 mm lateral, 1.8–2 mm posterior, 1.1 mm ventral. For PHA-L iontophoresis, 2.5% (by weight) PHA-L (Vector Labs, L-1110) solution in PBS, pH 8, was iontophoretically injected using current parameters 2 μA, alternating 7-s on, 7-s off, for 1 min with pipette tips broken to an outer diameter of 6–12 μm. For AAV iontophoresis, current parameters were 2 μA, 7-s on, 7-s off, for 2 min. Mice were perfused 5 (PHA-L) or 21 (AAV) days later and processed for PHA-L and Cre, or Cre, GFP, and mCherry immunostaining as described above. For entorhinal cortex axon tracing, CD-1 mice aged P40–P55 were used. AAV1-CMV–GFP (40–50 nl) was injected at 20 nl min$^{-1}$ into the coordinates (from bregma): medial entorhinal 2.8 mm lateral, 4.75 mm posterior, 2.75 mm ventral from brain surface; lateral entorhinal 4.6 mm lateral, 3.5 mm posterior, 3 mm ventral from brain surface. Mice were perfused 2 weeks later.

**Imaging and data analysis for CA1 axon tracing.** For whole-animal mutant tracing, every other 60-μm parasagittal section was stained and analysed. Images of injections were taken at 5× magnification on a Zeiss epiFluorescence scope and projections were imaged at 10×. Mice with labelling too faint to image or with retrogradely labelled cells were excluded. Images were acquired at identical gain and offset settings, but because injection and projection intensities varied between mice, exposure times were adjusted to avoid saturation. Fluorescence intensity measurements were taken on unprocessed images in FIJI and data were processed using custom MATLAB scripts. For quantification of injections, a 30-pixel-wide segmented line with spline fit was drawn along CA1, from proximal to distal. DAPI and Cre signals (from *Ten3$^{cre}$*) were used to identify the proximal end of CA1, and DAPI signal was used to identify the distal end of CA1. Intensity values along the CA1 line were measured using the Plot Profile command. For quantification of projections, a 180-pixel-wide segmented line with spline fit was drawn along the subiculum, from proximal to distal. The bottom of the line was aligned to the superficial border of subiculum pyramidal cell layer; the proximal border of subiculum was defined in the same way as the distal border of CA1: that is, the point where the compact CA1 cell body layer ended. The distal border of the subiculum was defined as the point where layer 2 of the presubiculum became obvious as an increase in DAPI density in the superficial cell body layer. The 180-pixel-wide curved line was straightened using the Straighten function under Selection. For injections that labelled CA2 and CA1, axons from CA2 were present near the distal border of CA1. Area selections were drawn around these axons and intensities were set to zero using the Clear function. Pixel values at each position were imported into MATLAB, and the 180 pixels for each point along the proximal–distal axis were averaged to give the fluorescence intensity at that coordinate of the proximal–distal axis. From this point forward, injections and projections were processed in the same way. A manual background subtraction was performed by selecting a value corresponding to an area of the trace that was only background signal, and this value was subtracted from all points on the trace. Any intensity values below zero after subtraction were set to 0. The length of the CA1 or subiculum axis was divided into 100 equally sized bins and intensity values were averaged within each bin. For each injection or projection, the three sections with the highest total labelling were combined by summing the three intensity values at each binned position. This summed intensity trace was then normalized to a peak value of 100. The mean position of the trace was calculated by multiplying the intensity value by the bin position, summing across the entire axis, and dividing by the sum of the intensity values. The width of the trace was defined as the full width-at-half-maximum. Traces were averaged across mice to produce the plots in Fig. 2e and Extended Data Fig. 5c, d, and the shaded error traces represent the standard error of the mean fluorescence intensity at that bin. For mean and width quantifications in Fig. 2f, g, the means were compared using two-tailed $t$-tests. For quantification of tracing across the proximal–distal axis of CA1 (Extended Data Fig. 5), injections and projections were processed as above. Values were combined into five groups for analysis and averaging based on the injection mean positions to the right of Extended Data Fig. 5d. Projection widths were compared using two-way analysis of variance (ANOVA) followed by a Šídák multiple comparisons test; multiplicity-adjusted $P$ values are reported. Projection mean regression lines were generated and compared using Prism 7 (GraphPad). All statistical analyses were performed in Prism 7 (GraphPad).

**Data analysis for conditional knockout experiments.** Tissue processing and imaging for CA1 and subiculum conditional knockout experiments were the same as for whole-animal mutants, with the following modifications. For subiculum conditional knockout, mice were excluded if lentivirus–GFP–Cre cells spread into the proximal half of CA1 (more than two cells in proximal CA1 per section, or if any PHA-L$^+$ cells were GFP–Cre$^+$). Some mice had GFP–Cre expression in the distal CA1; however, because these cells express low to no Ten3, these mice were included as subiculum conditional knockouts. GFP–Cre signal in subiculum was measured and quantified along with the PHA-L labelling intensity. Heatmaps were generated in MATLAB using the 'imagesc' function, and three-dimensional plots were generated in MATLAB using the 'surf' function. For CA1 conditional knockout, mice were excluded if lentivirus–GFP–Cre cells spread into the distal half of subiculum. The mRuby signal from AAV8-hSyn1-FLEx–mGFP–2a-synaptophysin–mRuby was used for injection quantifications and the mGFP for projection quantifications. In addition, we stained for Cre in the 647 nm channel instead of using the GFP–Cre signal, because of the presence of mGFP. mGFP and GFP–Cre signal could be unambiguously distinguished by staining for Cre. In cases where the GFP–Cre signal overlapped with the mGFP signal, the Cre staining in the 647 nm channel was used to mask out Cre$^+$ pixels, so the GFP–Cre signal was not counted as mGFP from CA1 axons. Analysis and quantification for CA1 conditional knockout projection mean and width was identical to the whole-animal knockout. For both CA1 and subiculum conditional knockouts, mice were excluded that had injection mean positions greater than 30 in CA1.

**Hippocampus cDNA sequencing.** Freshly dissected brains from P8 CD-1 mice were sliced horizontally into 1 mm slices using a tissue slicer. CA1 and subiculum were microdissected from individual slices using tungsten needles. Tissue from five mice was pooled, and total RNA was extracted using TRIzol reagent (Thermo Fisher, 15596018) and chloroform followed by purification using an RNeasy kit (Qiagen). DNA was removed by on-column digestion with DNase (Qiagen) for 15 min. cDNA was produced using a Superscript III First-Strand Synthesis System (Thermo Fisher, 18080-051) and a gene-specific primer located 3′ of splice site B (5′-ATCAGAGACGTACAAATCTCCGG-3′) followed by PCR for 30 cycles with Q5 polymerase (NEB) using the same primer and a primer located 5′ of splice site A: 5′-TGTAATCAGAGAGCTTGCCACC-3′. PCR products were cloned into pCR-Blunt II-TOPO (Thermo Fisher, 450245), individual colonies were miniprepped and sequenced using T7 and SP6 sequencing primers (Sequetech), and the status at splice sites A and B was assigned to individual clones using Geneious 10 software.

**DNA constructs.** Full-length mouse *Ten3* cDNA was obtained from Source Bioscience, clone identifier IRCKp5014M2020Q (accession number BC145284.1). This sequence lacks all alternatively spliced exons (corresponding to isoform $A_0B_0$). Haemagglutinin-tag was added and cDNA was cloned into pCDNA3.1(−) (Thermo Fisher, V79520) in two steps using a NEBuilder HiFi Assembly Kit (NEB, E2621) and NEB Stable competent cells (NEB, C3040H). Phusion Taq polymerase (NEB M0530) was used to amplify the 5′ portion for *Ten3* cDNA, adding a 5′ haemagglutinin-tag and Kozak sequence. Primers were as follows: 5′-TAGACT CGAGCGGCCGCCACCATGTACCCATACGATGTTCCAGATTACGCTGATG TGAAGGAACGCAGG-3′ and 5′-TGGAATTCTGCAGATATCCTGAGGAT CAGGCAA-3′. NEBuilder HiFi Assembly mix was used to insert this PCR fragment into pCDNA3.1(−) digested with EcoRV and NotI. The assembled product was subsequently digested with EcoRV and KpnI, and the HiFi Assembly mix was used to insert the 3′ end of Ten3 cDNA, amplified using the following primers: 5′-CCTGATCCTCAGGATATCATTAG-3′ and 5′-TTAAACTTAAGCT TGGTACCTTACCTCTTGCCGATCTCA-3′. The assembled product was fully sequenced. Additional isoforms were generated using a Q5 Site-Directed Mutagenesis Kit (NEB E0554S). $A_0B_1$ was generated from $A_0B_0$ using the following primers: 5′-TTAGACATAGTAGCAACCCAGCTCACAG-3′ and 5′-AATCTTT ATTTCTTAGTTCTAAAACACTTGTCACATTC-3′. $A_1B_0$ and $A_1B_1$ were generated from $A_0B_0$ and $A_0B_1$, respectively, using the following primers:

5′-AAGATAGTTAAAGAGGGTTGCCCCGGCTTGT-3′ and 5′-ATCCAAATAGTGAGCAATTGTGCAGTGCTCTCCGTTC-3′. $A_2B_1$ was generated from $A_1B_1$ using the following primers: 5′-GATATAAAGAGGGTTGCCCCGGCTTGT 3′ and 5′ CTATCTTGTCTTTAACTATCTTATCCAAATAGTGAGCAATTGTGCAG-3′. $A_3B_1$ was generated from $A_1B_1$ using the following primers: 5′-GGATATAAAGAGGGTTGCCCCGGCTTGT-3′ and 5′-TATCTTGTCTGCTTTAACTATCTTATCCAAATAGTGAGCAATTGTGCAG-3′.

All the haemagglutinin-tagged *Ten3*-isoform open reading frames were then cloned into a dual transcription unit vector under the Ef1α promoter. The vector also contained mCherry or GFP under the CMV promoter. Primers for amplifying the haemagglutinin-tagged open reading frames were 5′-TACAAAAAAGCAGGCTGCCACCGTCGACATGTACCCATACGATGTTC-3′ and 5′-TTGTACAAGAAAGCTGGGTGGATCCTTACCTCTTGCCGATC-3′. NEBuilder HiFi Assembly mix was used to insert this PCR fragment into the destination vector digested with BamHI and SalI. *CMV–mCherry* and *CMV–GFP* were generated by cloning eGFP and mCherry into NheI and HindIII-digested pCDNA3.1(−) using a NEBuilder HiFi Assembly Kit. eGFP and mCherry were amplified from source plasmids using the following primers: 5′-GGAGACCCAAGCTGGCTAGCCACCATGGTGAGCAAGGGCGA-3′ and 5′-ATCAGCGGTTTAAACTTAAGCTTTTACTTGTACAGCTCGTCCA-3′. The expression construct for human latrophilin-3 was published previously[54] and provided by R. Sando and T. Südhof.

**Single isoform K562 cell aggregation assay.** K562 cells (American Type Culture Collection (ATCC) CCL-243, lot 61978333) were grown in RPMI-1640 (Gibco 11875-093 with 10% FBS (Gibco A3160501) and 1× penicillin–streptomycin (Gibco 15140122). The lot was authenticated and tested for mycoplasma by ATCC. Cells were electroporated using a Neon Transfection system (Thermo Fisher MPK5000) with 100-μl tips. DNA was prepared using a HiPure Plasmid Filter MaxiPrep Kit (Thermo Fisher K210017). Fifteen micrograms of the Ef1α-Ten3 CMV–GFP dual transcription unit plasmid expressing a particular isoform were used for each electroporation. For the GFP-only condition, 6.43 μg of Ef1α-empty CMV–GFP along with 8.57 μg of empty pCDNA3.1 were used. Two million cells were washed once in 5 ml PBS, resuspended in 110 μl buffer R, mixed with DNA, and electroporated using the following settings: 1,450 V, 10 ms, three pulses, and added to 5 ml of warm RPMI-1640 with 10% FBS. Cells were incubated in six-well plates at 37 °C and 5% $CO_2$. Sixteen to 20 h later, cells were centrifuged at 200*g* for 3 min, resuspended in 1 ml RPMI-1640 + 10% FBS, and incubated for 15 min at 37 °C with 0.1 mg $ml^{-1}$ DNase (Worthington LS002060). Cells were washed twice with RPMI-1640 + 10% FBS, then resuspended in aggregation medium. Aggregation medium was neural growth medium: Neurobasal-A, 4% B27, 2 mM glutamine, 10% FBS, 20 mM HEPES. Cells were passed through a 40-μm cell strainer, counted, and added to wells of a 24-well plate at $4 \times 10^5$ cells per millilitre in 1 ml aggregation medium, and the plate was placed on a nutator at 37 °C for 1.5 h. After 1.5 h, cells were gently transferred to 2 ml of aggregation media in a six-well plate and imaged with a Nikon Eclipse Ti microscope using a 4× lens. Five images were taken for each well. Images were thresholded in FIJI, and Analyze Particles was used to measure particle number and size. Particle sizes from three separate experiments were combined, and particles below 600 $\mu m^2$, the size of a large $GFP^+$ cell in control wells, were filtered out to remove single cells. Combined particle sizes were then compared with GFP-only control using a Kruskal–Wallis test followed by Dunn's multiple comparisons test. A family-wide significance level was set to 0.05, and multiplicity-adjusted *P* values were reported. For haemagglutinin immunostaining following aggregation, cells were fixed in 4% paraformaldehyde for 15 min, centrifuged for 3 min at 200*g*, rinsed once with PBS, and resuspended in 30% sucrose in PBS. Cells were spun onto Superfrost Plus slides using a cytospin[55] then incubated in the following solutions, at room temperature except for primary antibody: 2 × 5 min in PBS, 10 min in 0.1% Triton X-100 in PBS, 3 × 5 min in PBS, 30 min in 10% NDS in PBS, overnight in primary antibody (Ms anti-haemagglutinin, Covance MMS-101R) at 4 °C in 5% NDS in PBS, 3 × 5 min in PBS, 2 h in secondary antibody (Donkey Alexa 647 anti-mouse, Jackson ImmunoResearch) in 5% NDS in PBS, 3 × 5 min in PBS, 5 min in DAPI, and 5 min in PBS. Aggregates were imaged at 40× magnification on a Zeiss 780 confocal microscope.

**K562 mixed cell aggregation assay.** For the Ten3 isoform mixing assay (Extended Data Fig. 10), electroporations and aggregation assay were performed as above with the following modifications. The mCherry versions of the dual promoter constructs were used where appropriate. The two populations of cells were mixed at $2 \times 10^5$ each in 1 ml aggregation media, for a final cell concentration of $4 \times 10^5$ cells per millilitre. Phase-contrast images of the cells and aggregates were also taken. For quantification, aggregates were identified from the phase image, then identified as mixed, GFP-only, or mCherry-only, on the basis of the merged fluorescence image. Mixed aggregates had to contain at least three cells of each colour, to avoid identifying single population aggregates as mixed because of chance overlap with a single cell in the other channel. At least 100 aggregates across three separate experiments were counted. For the latrophilin-3 and Ten3 mixing experiment, conditions and analysis differed as described below. For each electroporation, 5 μg CMV–GFP DNA was co-electroporated with 12 μg CMV-Ten3 or 12 μg empty pCDNA3.1, or 5 μg CMV–mCherry and 1.75 μg CMV-latrophilin-3. Aggregation media were the same as above except with 1.25% FBS rather than 10%. After 1.5 h of mixing, 3 μl aliquots were taken from the wells, spotted onto slides, and imaged at 5× magnification on a Zeiss epifluorescence scope. Three or four aliquots were taken per well, and two images were taken per aliquot. For aggregate size quantification, the GFP and mCherry channels were thresholded, combined, and Analyze Particles was used on the combined binary image to measure particle number and size. Particle sizes from three separate experiments were combined, and particles below a 600 $\mu m^2$, the size of a large $GFP^+$ cell in control wells, were filtered out to remove single cells. Combined particle sizes were then compared with latrophilin-3 and GFP-only control using a Kruskal–Wallis test followed by Dunn's multiple comparisons test. A family-wide significance level was set to 0.05, and multiplicity-adjusted *P* values were reported.

**Code availability.** Custom MATLAB scripts used in analysing data are available from the corresponding author upon reasonable request.

**Data availability.** All data supporting the findings reported in this study are available from the corresponding author upon reasonable request. The Ten3 isoform cDNA sequences have been deposited in GenBank under accession numbers MG387139–MG387146.


51. Tasic, B. *et al.* Site-specific integrase-mediated transgenesis in mice via pronuclear injection. *Proc. Natl Acad. Sci. USA* **108,** 7902–7907 (2011).
52. Weissbourd, B. *et al.* Presynaptic partners of dorsal raphe serotonergic and GABAergic neurons. *Neuron* **83,** 645–662 (2014).
53. Beier, K. T. *et al.* Circuit architecture of VTA dopamine neurons revealed by systematic input-output mapping. *Cell* **162,** 622–634 (2015).
54. Lu, Y. C. *et al.* Structural basis of latrophilin-FLRT-UNC5 interaction in cell adhesion. *Structure* **23,** 1678–1691 (2015).
55. Sisino, G., Bellavia, D., Corallo, M., Geraci, F. & Barbieri, R. A homemade cytospin apparatus. *Anal. Biochem.* **359,** 283–284 (2006).
56. Witter, M. in *The Mouse Nervous System* (eds Watson, C., Paxinos, G. & Puelles, L.) 112–139 (Elsevier, 2012).
57. Kohara, K. *et al.* Cell type-specific genetic and optogenetic tools reveal hippocampal CA2 circuits. *Nat. Neurosci.* **17,** 269–279 (2014).
58. Caballero-Bleda, M. & Witter, M. P. Regional and laminar organization of projections from the presubiculum and parasubiculum to the entorhinal cortex: an anterograde tracing study in the rat. *J. Comp. Neurol.* **328,** 115–129 (1993).
59. Honda, Y. & Ishizuka, N. Organization of connectivity of the rat presubiculum: I. efferent projections to the medial entorhinal cortex. *J. Comp. Neurol.* **473,** 463–484 (2004).
60. O'Reilly, K. C., Gulden Dahl, A., Ulsaker Kruge, I. & Witter, M. P. Subicular–parahippocampal projections revisited: development of a complex topography in the rat. *J. Comp. Neurol.* **521,** 4284–4299 (2013).
61. Wright, N. F., Vann, S. D., Erichsen, J. T., O'Mara, S. M. & Aggleton, J. P. Segregation of parallel inputs to the anteromedial and anteroventral thalamic nuclei of the rat. *J. Comp. Neurol.* **521,** 2966–2986 (2013).
62. Meibach, R. C. & Siegel, A. Efferent connections of the hippocampal formation in the rat. *Brain Res.* **124,** 197–224 (1977).
63. Ishizuka, N. Laminar organization of the pyramidal cell layer of the subiculum in the rat. *J. Comp. Neurol.* **435,** 89–110 (2001).
64. Wright, N. F., Erichsen, J. T., Vann, S. D., O'Mara, S. M. & Aggleton, J. P. Parallel but separate inputs from limbic cortices to the mammillary bodies and anterior thalamic nuclei in the rat. *J. Comp. Neurol.* **518,** 2334–2354 (2010).

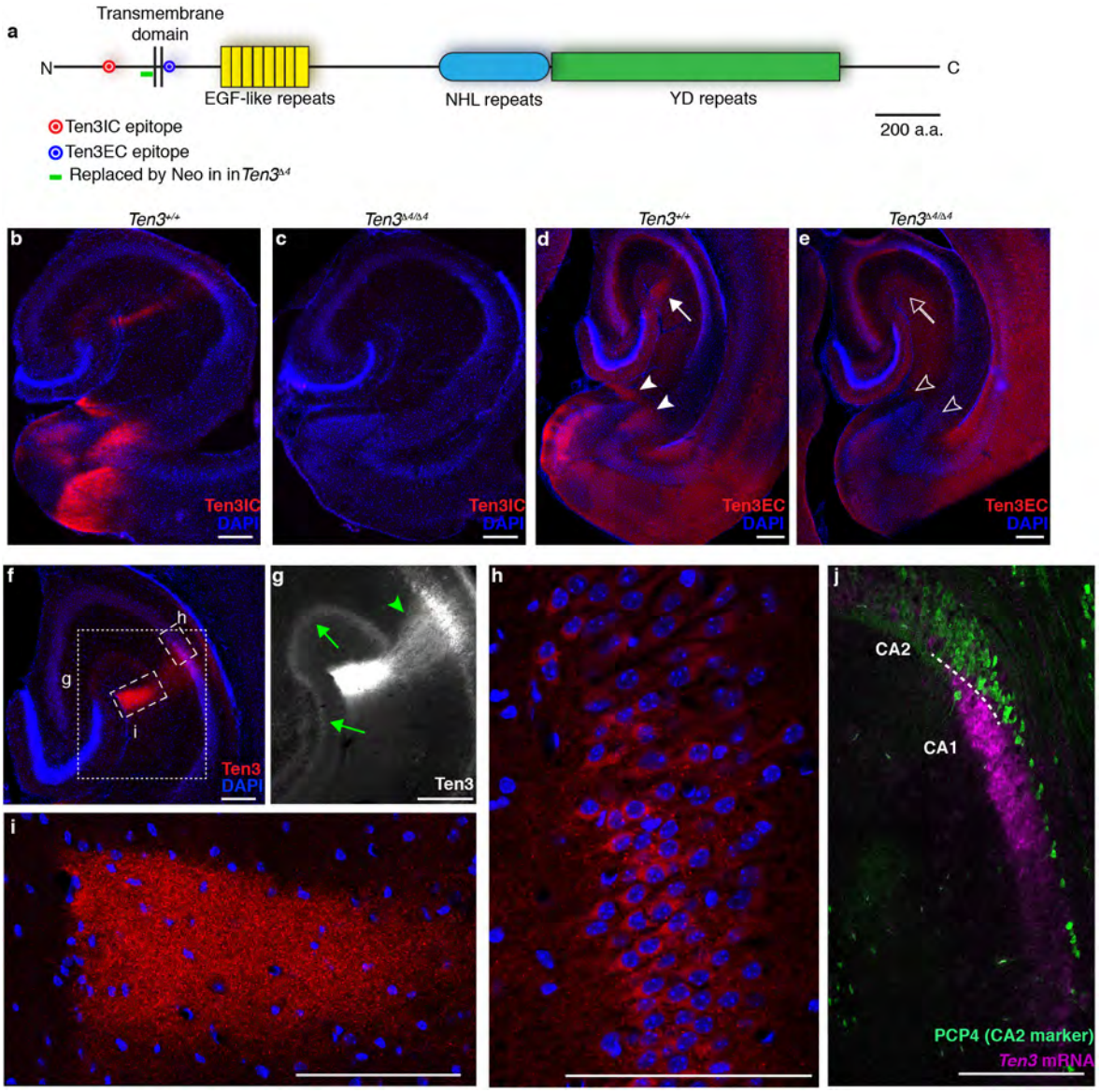


**Extended Data Figure 1 | Ten3 staining details and controls. a**, Diagram of Ten3 protein showing location of antibody epitopes, specific domains, and region deleted in the $Ten3^{\Delta 4}$ mutant. In $Ten3^{\Delta 4}$, a neomycin resistance cassette (Neo) replaces 110 base pairs of sequence directly N-terminal to the transmembrane domain. The Ten3IC antibody was used for all Ten3 stainings in the paper except **d** and **e** of this figure. Scale bar, 200 amino acids. **b**, **c**, Ten3IC staining (red) on P9 horizontal sections of $Ten3^{WT}$ (**b**) and mutant $Ten3^{\Delta 4/\Delta 4}$ (**c**) brains, showing loss of staining in *Ten3* mutants. Note that the Ten3IC epitope is located N-terminal to Δ4, suggesting that in $Ten3^{\Delta 4/\Delta 4}$ either the mRNA undergoes nonsense-mediated decay or the truncated protein is not stable. **d**, **e**, Ten3EC staining on P10 horizontal sections of $Ten3^{WT}$ (**d**) and mutant $Ten3^{\Delta 4/\Delta 4}$ (**e**) brains. Staining has a higher background than Ten3IC antibody, but signal is present in proximal CA1 (arrow) and distal subiculum (arrowheads), similar to Ten3IC, which is absent in the knockout (open arrow/arrowheads). **f**, Ten3 staining (red) on P10 horizontal section with boxes around regions magnified in **g**–**i**. **g**, Ten3 staining in dentate gyrus from **f**, CA3, and CA1. Intensity was increased to highlight Ten3 signal in axons and dendrites. Ten3 in stratum radiatum of proximal CA1 (arrowhead) is most probably from CA1 dendrites, since CA3 cells, the major source of axons in this layer, did not express *Ten3* mRNA (Fig. 1b). Ten3 in the molecular layers of dentate gyrus and CA3 (arrows) is probably contributed by the axons of MEC layer II neurons[56], since dentate gyrus and CA3 neurons did not express *Ten3* mRNA (Fig. 1b). **h**, Proximal CA1 pyramidal cell layer from **f**, showing Ten3 signal in cell bodies. **i**, Proximal CA1 stratum lacunosum-moleculare from **f**, showing Ten3 signal in the region where MEC axons synapse onto CA1 pyramidal neuron dendrites. **j**, *In situ* hybridization on P9 horizontal section for *Ten3* mRNA (magenta) combined with immunostaining for PCP4 (green), a marker of CA2 neurons[57]. No overlap between Ten3 and PCP4 was observed. Scale bars, 200 μm in **b**–**g**, **j**, and 100 μm in **h**, **i**.

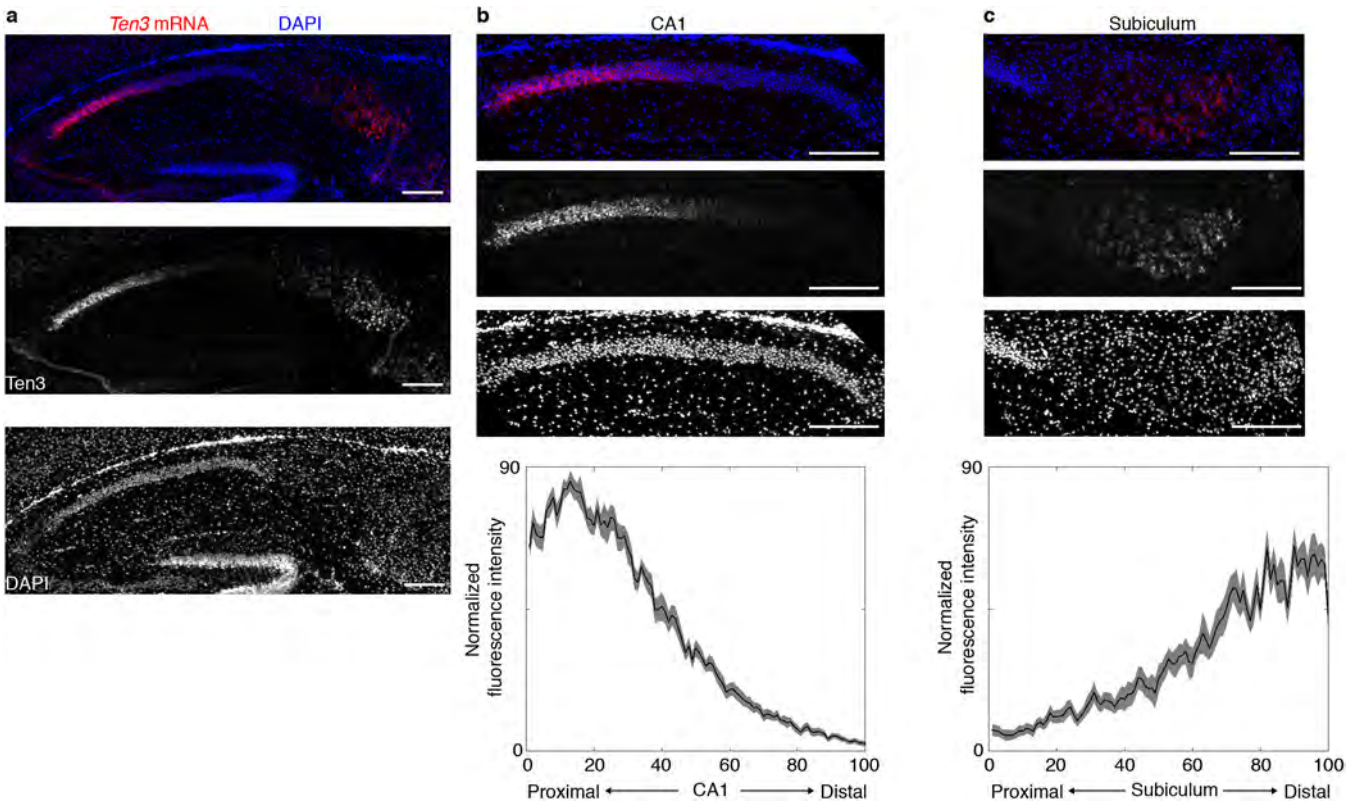


**Extended Data Figure 2 | Distribution of *Ten3* mRNA in sagittal sections. a**, *In situ* hybridization for *Ten3* mRNA on sagittal section of P10 brain. Top, merged image with *Ten3* mRNA signal in red and DAPI in blue; middle, *Ten3* mRNA signal alone; bottom: DAPI signal alone. **b**, Top: magnified image of *Ten3 in situ* hybridization in CA1; bottom: quantification of *Ten3* mRNA along the proximal–distal axis of CA1 ($n = 12$ sections, four mice), showing a graded signal that peaks in proximal CA1 and decreases to a minimum in distal CA1. Proximal–distal axis is divided into 100 bins, with 1 being most proximal and 100 most distal. Shaded curves represent mean ± s.e.m. **c**, Top: magnified image of *Ten3 in situ* hybridization in subiculum; bottom: quantification of *Ten3* mRNA along the proximal–distal axis of subiculum ($n = 14$ sections, four mice) showing a graded signal that peaks in distal subiculum and decreases to a minimum in proximal subiculum. The distributions in CA1 and subiculum are similarly shaped but reversed along the proximal–distal axis, reflecting the graded topographic connections along this axis (see Fig. 2 and Extended Data Fig. 5c). Scale bars, 200 μm in all panels.

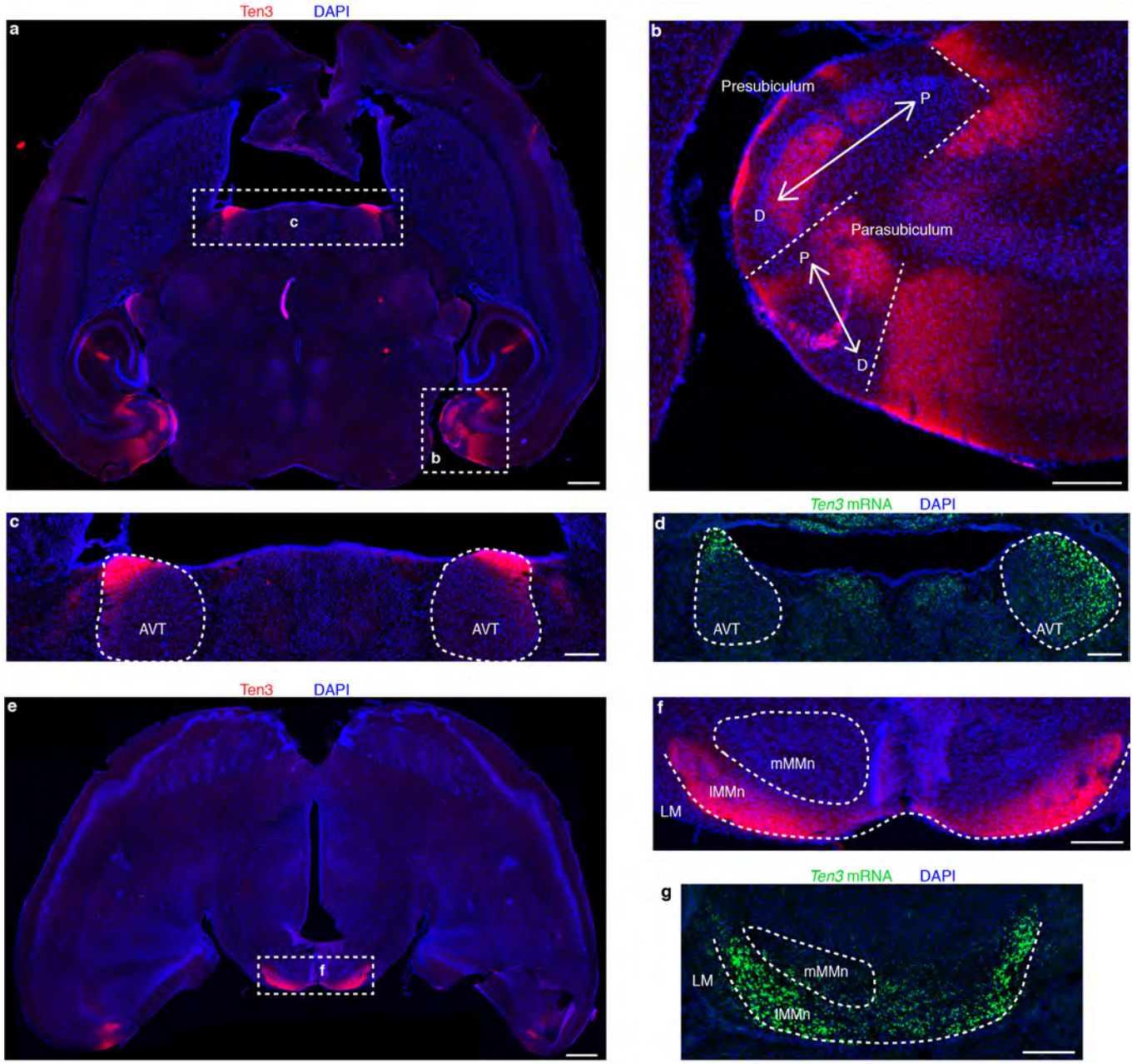


**Extended Data Figure 3 | Ten3 expression and topography details.** **a**, Ten3 staining (red) on P10 horizontal section. Dotted rectangles highlight staining in the hippocampal region and anteroventral thalamic nucleus, which are magnified in **b** and **c**. **b**, The parahippocampal region from **a**, showing expression of Ten3 relative to the proximal–distal (P–D) axes (arrows) in the presubiculum and parasubiculum. The connectivity of these regions is complex[58,59], but seems to be consistent with preferential connectivity between Ten3-expressing subregions. Ten3 is expressed in distal presubiculum (close to parasubiculum), which projects to MEC near the parasubicular border[59], and receives projections from distal subiculum[60], both Ten3-high subregions. Ten3 is also expressed in proximal parasubiculum, which projects to MEC[58] and receives projections from distal subiculum[60], again both Ten3-high subregions. **c**, The anteroventral thalamus from **a**, showing intense Ten3 staining in the anterior and lateral division of the anteroventral thalamic nucleus (AVT, outlined). Distal subiculum, another Ten3-high region, projects to the anteroventral thalamic nucleus, whereas proximal subiculum projects to the anteromedial thalamus[61]. **d**, *In situ* hybridization for *Ten3* mRNA (green) on P9 horizontal section from similar location as **c**. **e**, Ten3 staining (red) on P10 horizontal section, more ventral than **a**. Dotted rectangle highlights intense staining in the medial mammillary nucleus, which is magnified in **f**. **f**, Medial mammillary nucleus from **e**, showing Ten3 labelling in the lateral division of the medial mammillary nucleus (lMMn). Outlines show location of lateral mammillary nucleus (LM), lateral division of the medial mammillary nucleus, and medial division of the medial mammillary nucleus (mMMn). Proximal subicular neurons project to the medial division of the medial mammillary nucleus, whereas Ten3-high distal subicular neurons project to the Ten3-high lateral division[40,62–64]. The neurons of the lateral division project to the Ten3-high anteroventral thalamic nucleus, while medial division neurons project to the anteromedial thalamic nucleus[61]. **g**, *In situ* hybridization for *Ten3* mRNA (green) on P9 horizontal section from similar location as **f**. Scale bars, 500 μm in **a** and **e**; 200 μm elsewhere. In summary, the pattern of Ten3-high to Ten3-high connectivity observed for CA1, subiculum, and entorhinal cortex seems to extend to many of the topographic projections formed between these subregions and the presubiculum, parasubiculum, thalamus, and mammillary nucleus.

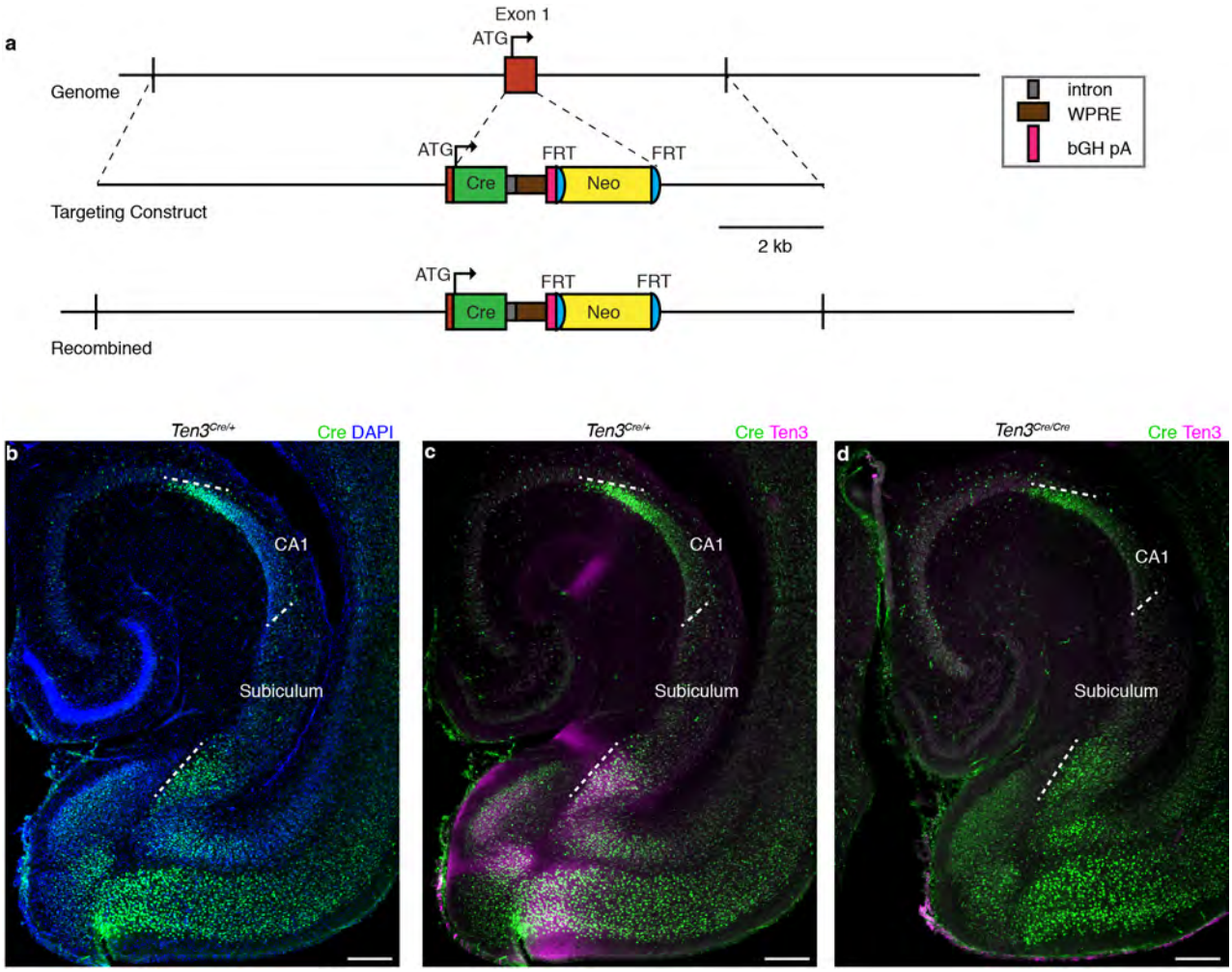


**Extended Data Figure 4 | Generation and characterization of *Ten3$^{cre}$*.** **a**, Design of *Ten3$^{cre}$*. Top: region of chromosome 8 containing *Ten3* exon 1, which contains the start codon (ATG). Middle: targeting construct with *cre* open reading frame inserted directly after the Ten3 start codon. *cre* is followed by a synthetic intron, woodchuck hepatitis virus post-transcriptional regulatory element (WPRE), and bovine growth hormone polyadenylation sequence (bGH pA) (see key on right). Neo includes a phosphoglycerate kinase (PGK) promoter driving the resistance gene. Bottom: genomic region after homologous recombination. The endogenous exon 1 sequence after the start codon is replaced with *cre*. Neo was not removed by flippase (FLP)-mediated recombination in the mice used in Fig. 2. **b**–**d**, Cre and Ten3 protein expression in P10 horizontal sections from *Ten3$^{cre}$* mice. White dotted lines highlight proximal and distal borders of CA1 and subiculum. **b**, **c**, Cre expression (green) mimics the distribution of Ten3 expression (magenta) in *Ten3$^{Het}$* mice. **d**, In *Ten3$^{cre/cre}$* mice, Ten3 immunostaining is absent. Scale bars, 200 μm.

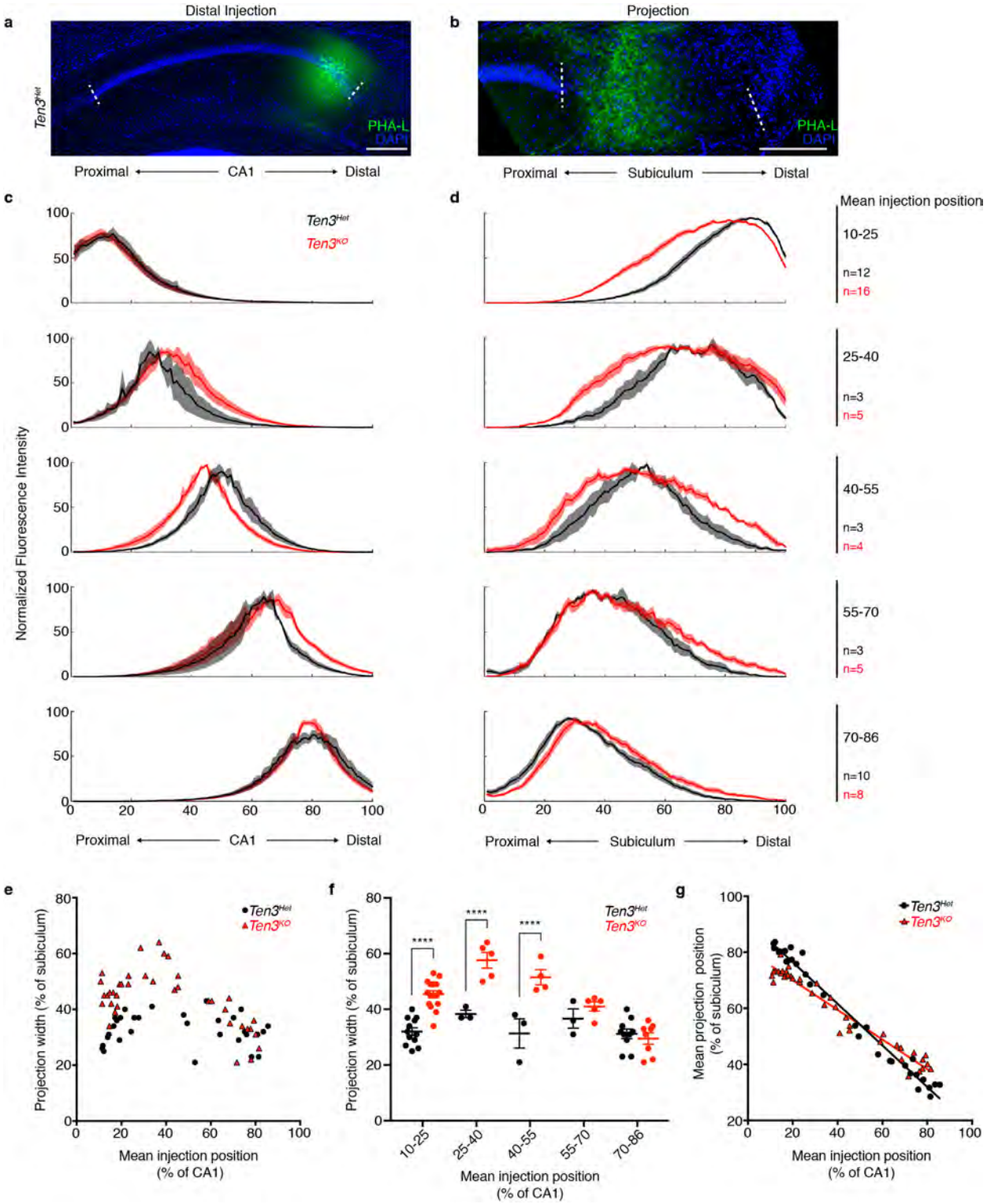


**Extended Data Figure 5 | Analysis of CA1→subiculum projections with various injection sites in *Ten3*$^{Het}$ control and *Ten3*$^{KO}$ mice.** **a**, **b**, PHA-L (green) injection in distal CA1 (**a**) and corresponding projection in proximal subiculum (**b**) in *Ten3*$^{Het}$ mouse. Scale bars, 200 μm. **c**, **d**, Averaged normalized injection (**c**) and projection (**d**) traces of all *Ten3*$^{Het}$ (black) and *Ten3*$^{KO}$ (red) mice analysed, binned into five groups by the mean position of the injection, and plotted from most proximal (top) to most distal (bottom) injections (bin limits and number of mice per bin listed on the right of **d**). Proximal–distal axis position is numbered from 1 (most proximal) to 100 (most distal). Shaded error curves represent mean ± s.e.m. at each bin. **e**, Projection width in subiculum versus injection mean position in CA1 for all mice (*Ten3*$^{Het}$: $n = 31$, black circles; *Ten3*$^{KO}$: $n = 38$, red triangles). **f**, Projection width data binned by injection mean. Number of mice per bin same as **d**. Projection width was significantly increased in *Ten3*$^{KO}$ for the three most proximal bins. ****$P < 0.0001$; multiplicity-adjusted $P$ values after two-way ANOVA with Šídák's correction for multiple comparisons. Error bars, mean ± s.e.m. **g**, Projection mean position in subiculum versus injection mean position in CA1 for all mice used (*Ten3*$^{Het}$: $n = 31$; *Ten3*$^{KO}$: $n = 38$), with superimposed linear regression lines (*Ten3*$^{Het}$: $R^2 = 0.9812$; *Ten3*$^{KO}$: $R^2 = 0.9515$). The slopes were significantly different ($P < 0.0001$), indicating a less sharp topography in *Ten3*$^{KO}$ mice. Bin 1 data (most proximal, injection mean 10–25) in **c**–**g** are the same data as in Fig. 2e–g.

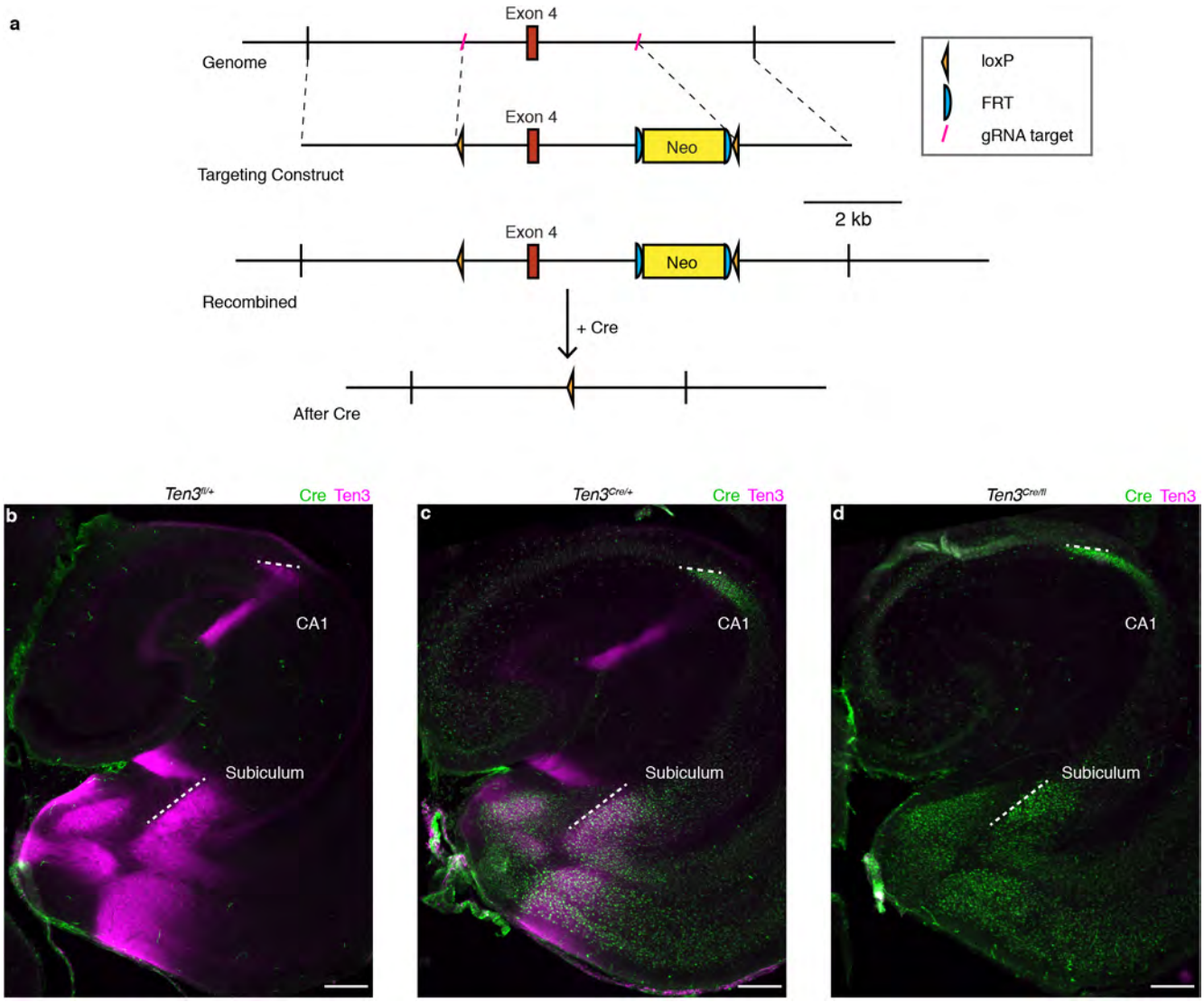


**Extended Data Figure 6 | Generation and characterization of *Ten3$^{flox}$*.** **a**, Design of *Ten3$^{fl}$*. Top: region of chromosome 8 containing Ten3 exon 4, which is 239 base pairs long and encodes 19 of the 21 amino acids in the transmembrane domain. Guide RNA (gRNA) targets shown in red (see key at right). Line 2: targeting construct with *loxP* sites inserted 5′ and 3′ of exon 4. Neo includes a PGK promoter driving the resistance gene. Line 3: genomic region after homology-directed repair. Bottom: deletion of exon 4 after Cre-mediated recombination between *loxP* sites. Neo was removed by FLP-mediated recombination in some of the mice used in Figs 3 and 4. In addition to deleting exon 4, the reading frame 3′ to exon 4 is frame-shifted with respect to the reading frame 5′ to exon 4. **b**–**d**, Cre (green) and Ten3 (magenta) protein expression in P10 horizontal sections from *Ten3$^{fl/+}$* (**b**), *Ten3$^{Het}$* (**c**), and *Ten3$^{cre/fl}$* (**d**) mice. Ten3 staining is absent in *Ten3$^{cre/fl}$* mice. White dotted lines highlight proximal and distal borders of CA1 and subiculum. Scale bars, 200 μm.

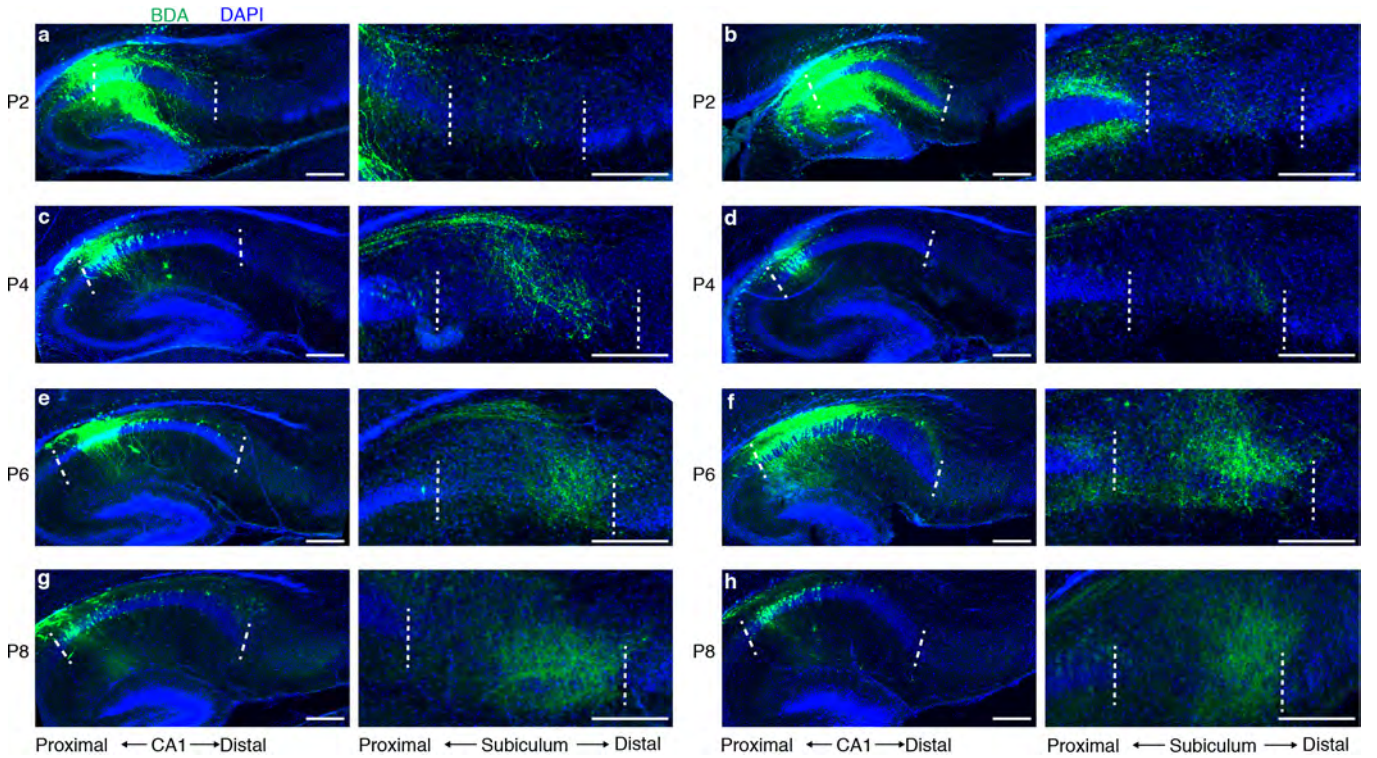


**Extended Data Figure 7 | Time course of CA1→subiculum projection development.** Sagittal sections from mice injected with BDA (green) in CA1 at P0, and perfused for staining at P2 (**a**, **b**), P4 (**c**, **d**), P6 (**e**, **f**), or P8 (**g**, **h**). Two mice are shown for each time point with a pair of images per mouse. Within each pair, the left image shows the section that contains the centre of the injection site at CA1, whereas the right image shows a magnified image of the section containing the highest density of projection at subiculum. Dashed lines mark proximal and distal CA1 borders in the left panels, and proximal and distal subicular borders in the right panels. CA1 axons are largely absent at subiculum at P2, and increase intensity from P4 to P8. Scale bars, 200 μm.

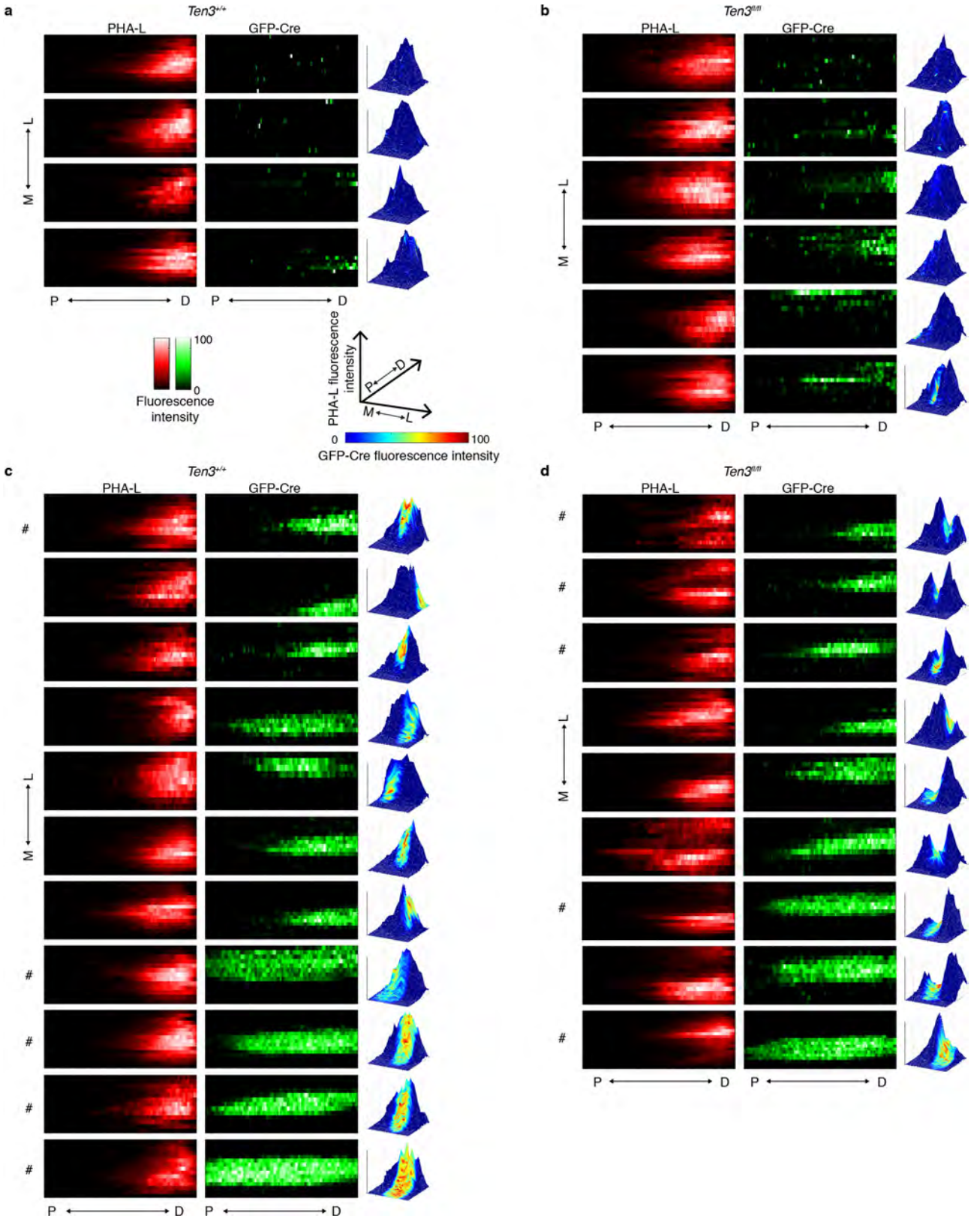


**Extended Data Figure 8 | Subiculum conditional knockout plots.** **a**, **b**, Plots from *Ten3*$^{WT}$ (**a**) and *Ten3*$^{fl/fl}$ (**b**) mice with minimal GFP–Cre expression. Heatmaps show normalized PHA-L fluorescence intensity (red, left) and normalized GFP–Cre intensity (green, middle) in subiculum, same mice. Each row is one section, 120 μm between rows, colour bars shown below **a**, and proximal–distal position is on the *x* axis. Surface plots are to the right of the corresponding heatmaps, showing PHA-L fluorescence intensity as height and GFP–Cre fluorescence intensity according to the colour map shown below **a**. P, proximal; D, distal; M, medial; L, lateral. Projections are similar between *Ten3*$^{WT}$ and *Ten3*$^{fl/fl}$. **c**, **d**, Plots from *Ten3*$^{WT}$ (**c**) and *Ten3*$^{fl/fl}$ (**d**) mice with high GFP–Cre expression in subiculum. In *Ten3*$^{fl/fl}$ mice, PHA-L signal is decreased in GFP–Cre regions. Number of mice shown in Fig. 4.

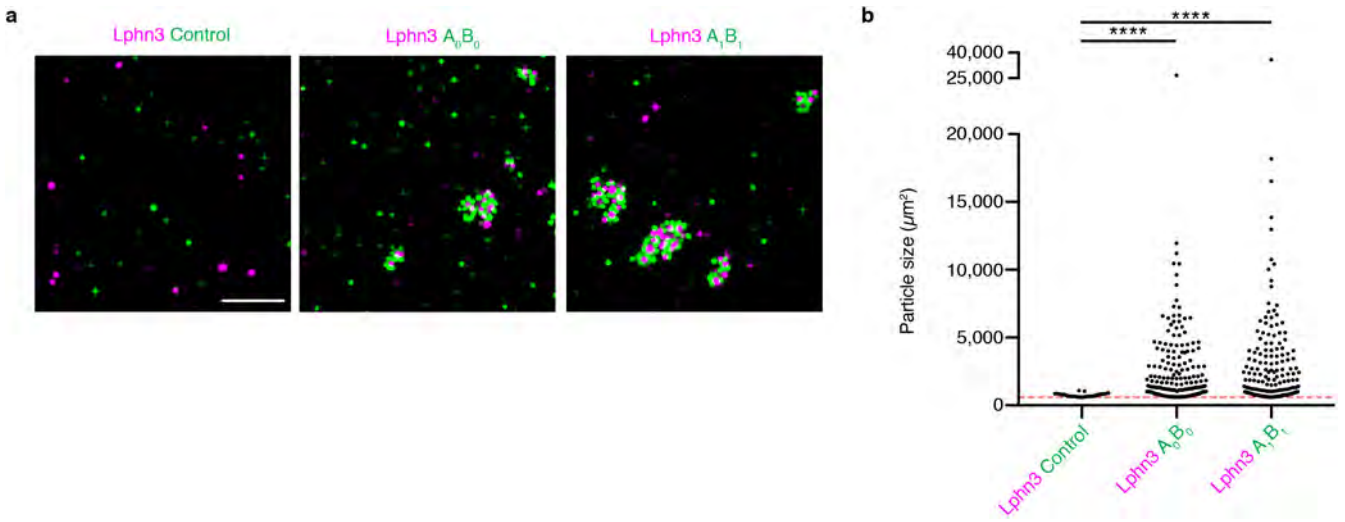


**Extended Data Figure 9 | Latrophilin-3 and Ten3 aggregation assay. a**, Images from aggregation assay with cells co-transfected with latrophilin-3 (Lphn3) and mCherry (magenta) mixed with cells co-transfected with GFP and empty vector (left), $A_0B_0$ isoform of Ten3 (middle), or $A_1B_1$ isoform of Ten3 (right). Scale bar, 200 μm, applies to all images. **b**, Quantification of aggregate sizes pooled from three biological replicates. Dashed red line shows cutoff at 600 $\mu m^2$, the size of a large $GFP^+$ cell from the control images. Asterisks denote significance from Dunn's multiple comparisons test after a Kruskal–Wallis test, comparing all conditions with the Lphn3 and control mix, Lphn3 + control: $n = 32$ particles above threshold; Lphn3 + $A_0B_0$: $n = 172$; Lphn3 + $A_1B_1$: $n = 159$. NS, not significant; $^{****}P \leq 0.0001$, multiplicity-adjusted $P$ values.

a

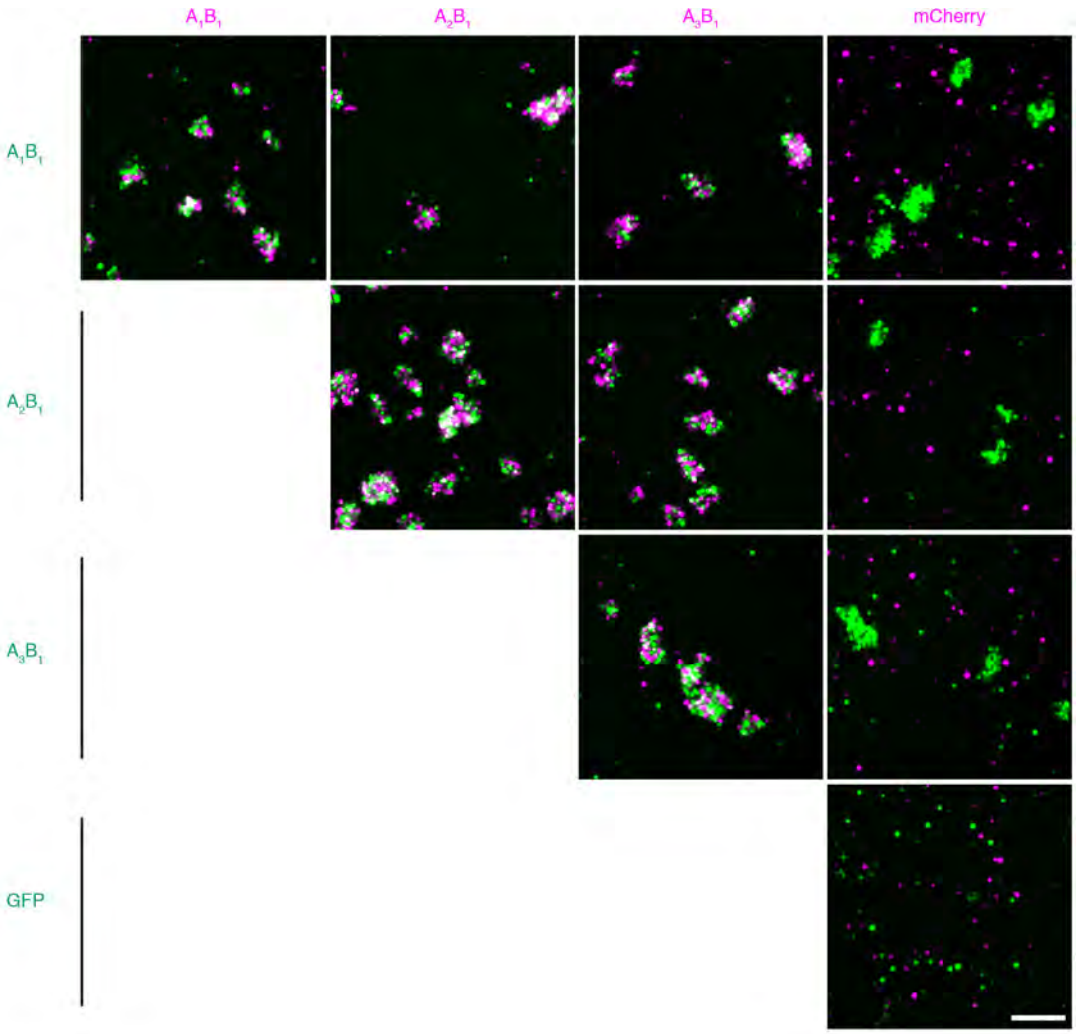


b

| GFP + | mCherry + $A_1B_1$ | mCherry + $A_2B_1$ | mCherry + $A_3B_1$ | mCherry only |
|---|---|---|---|---|
| $A_1B_1$ | 100% mixed (110/110) | 100% mixed (113/113) | 100% mixed (100/100) | 97.1% GFP only (102/105)<br>2.9% mCherry only (3/105) |
| $A_2B_1$ | | 100% mixed (110/110) | 100% mixed (113/113) | 100% GFP only (100/100) |
| $A_3B_1$ | | | 100% mixed (109/109) | 100% GFP only (103/103) |
| GFP only | | | | 0 aggregates observed |

**Extended Data Figure 10 | Aggregation assays for cells expressing different Ten3 splicing isoforms. a**, Cell aggregation assay with combinations of K562 cells expressing the $A_1B_1$, $A_2B_1$, or $A_3B_1$ Ten3 isoform along with GFP or mCherry. Scale bar in bottom right panel, 200 μm, applies to all images. **b**, Quantification of aggregates observed in three biological replicates of the aggregation experiment in **a**. At least 100 aggregates were counted across the three replicates in each of the 10 mixing conditions, except for the GFP-alone and mCherry-alone controls, where no aggregates were observed. One hundred per cent of aggregates were mixed in combinations where both cell populations expressed a Ten3 isoform. No mixed aggregates were observed in combinations of Ten3-expressing cells with cells expressing mCherry alone, confirming that the aggregation is Ten3-dependent and not due to an endogenously expressed interaction partner. Fractions in parentheses indicate aggregates of a particular type out of all aggregates counted in that condition.

nature research

Corresponding author(s): Liqun Luo

☐ Initial submission ☐ Revised version ☒ Final submission

# Life Sciences Reporting Summary

Nature Research wishes to improve the reproducibility of the work that we publish. This form is intended for publication with all accepted life science papers and provides structure for consistency and transparency in reporting. Every life science submission will use this form; some list items might not apply to an individual manuscript, but all fields must be completed for clarity.

For further information on the points included in this form, see Reporting Life Sciences Research. For further information on Nature Research policies, including our data availability policy, see Authors & Referees and the Editorial Policy Checklist.

## Experimental design

1. Sample size

   Describe how sample size was determined.

   No statistical methods were used to determine sample size, but sample sizes are similar to those generally used in the field. > 8-10 animals per genotype for tracing and n=3 for aggregation experiments

2. Data exclusions

   Describe any data exclusions.

   For tracing experiments, animals were excluded if axons/injections were not visible. For CA1 cKO experiment, animals were excluded if lentivirus spread into distal half of subiculum. For Subiculum cKO, animals were excluded if lentivirus spread into proximal half of CA1. For aggregation experiments, different conditions were tested before settling on final protocol; only results from the final protocol are included here. For developmental BDA tracing, animals were excluded where the injections missed or spread into subiculum.

3. Replication

   Describe whether the experimental findings were reliably reproduced.

   All attempts at replication were successful. All animals with successful tracing are included here, so the variability of the tracing results is evident from the main figures.

4. Randomization

   Describe how samples/organisms/participants were allocated into experimental groups.

   No randomization was used. Within litters, animals received the same injections regardless of genotype.

5. Blinding

   Describe whether the investigators were blinded to group allocation during data collection and/or analysis.

   Experiments were blind to genotype during injection and data collection. No blinding was used for in vitro experiments or electrophysiology.

Note: all studies involving animals and/or human research participants must disclose whether blinding and randomization were used.

6. Statistical parameters

For all figures and tables that use statistical methods, confirm that the following items are present in relevant figure legends (or in the Methods section if additional space is needed).

| n/a | Confirmed |
|---|---|
| ☐ | ☒ The exact sample size (*n*) for each experimental group/condition, given as a discrete number and unit of measurement (animals, litters, cultures, etc.) |
| ☐ | ☒ A description of how samples were collected, noting whether measurements were taken from distinct samples or whether the same sample was measured repeatedly |
| ☐ | ☒ A statement indicating how many times each experiment was replicated |
| ☐ | ☒ The statistical test(s) used and whether they are one- or two-sided (note: only common tests should be described solely by name; more complex techniques should be described in the Methods section) |
| ☐ | ☒ A description of any assumptions or corrections, such as an adjustment for multiple comparisons |
| ☐ | ☐ The test results (e.g. *P* values) given as exact values whenever possible and with confidence intervals noted |
| ☐ | ☒ A clear description of statistics including central tendency (e.g. median, mean) and variation (e.g. standard deviation, interquartile range) |
| ☐ | ☒ Clearly defined error bars |

*See the web collection on statistics for biologists for further resources and guidance.*

## Software

Policy information about availability of computer code

7. Software

| | |
|---|---|
| Describe the software used to analyze the data in this study. | Statistics and plotting were performed using Prism 7 from Graphpad. FIJI/ImageJ was used for image analysis in combination with custom MATLAB code, which is available upon request. Geneious 10 software was used for sequence analysis of cDNA clones. pClamp 10 was used for analyzing electrophysiology signals. |

For manuscripts utilizing custom algorithms or software that are central to the paper but not yet described in the published literature, software must be made available to editors and reviewers upon request. We strongly encourage code deposition in a community repository (e.g. GitHub). *Nature Methods* guidance for providing algorithms and software for publication provides further information on this topic.

## Materials and reagents

Policy information about availability of materials

8. Materials availability

| | |
|---|---|
| Indicate whether there are restrictions on availability of unique materials or if these materials are only available for distribution by a for-profit company. | Unique materials, including antibodies, transgenic mouse lines, and plasmids, are available from the authors upon request. |

9. Antibodies

Describe the antibodies used and how they were validated for use in the system under study (i.e. assay and species).

The following are commonly used commercially available antibodies. Specificity was validated by staining in controls lacking the antigen or, for axon tracing, by comparing signal in non-injected areas to injected areas.
Chicken anti-GFP Aves Labs GFP-1020. used at 1:2500. Multiple lot #s, not recorded.
Rat anti-mCherry clone 16D7 ThermoFisher M11217, used at 1:1000. Lot #: RI240561 and QE214609.
Mouse anti-Cre clone 2D8 Millipore MAB3120, used at 1:1000. Specificity control, see Extended Data Fig. 4c vs 4b. Multiple lot #s, not recorded.
Rabbit anti-PHAL Vector Labs AS-2300, used at 1:1000. Multiple lot #s, not recorded.
Mouse anti-HA.11 clone 16B12 Covance MMS101R. Used at 1:1000, lot number not recorded. Specificity confirmed by lack of staining on cells not transfected with HA expressing plasmid (data not shown).
Secondary antibodies are commonly used reagents from Jackson Immunoresearch. Specificity was validated by lack of signal in samples lacking primary antibody or in brain regions lacking the antigen recognized by the primary antibody.
Cy3 Donkey anti-Rabbit 711-165-152
488 Donkey anti-Rabbit 711-545-152
488 Donkey anti-Mouse 715-545-151
647 Donkey anti-Mouse 715-605-150
488 Donkey anti-Chicken 703-545-155
Cy3 Donkey anti-Rat 712-165-150

The following custom antibodies were used, and validated by immunostaining on brain tissue from previously published Teneurin-3 knockout mice - see Extended Data Fig. 2.
Rabbit anti-Ten3IC, against amino acids 163-176
Rabbit anti-Ten3EC, against amino acids 346-364

10. Eukaryotic cell lines

a. State the source of each eukaryotic cell line used.

K562 cells were obtained from ATCC: ATCC CCL-243, Lot 61978333

b. Describe the method of cell line authentication used.

We did not authenticate the cell line our lab. The lot was authenticated by ATCC before shipment.

c. Report whether the cell lines were tested for mycoplasma contamination.

We did not test for mycoplasma contamination in our lab. The lot was tested at ATCC before shipment.

d. If any of the cell lines used are listed in the database of commonly misidentified cell lines maintained by ICLAC, provide a scientific rationale for their use.

No commonly misidentified cell lines were used.

## Animals and human research participants

Policy information about studies involving animals; when reporting animal research, follow the ARRIVE guidelines

11. Description of research animals

Provide details on animals and/or animal-derived materials used in the study.

As reported in methods, all expression studies were performed on CD-1 mice from Charles River and both sexes were used. Ages of CD-1 animals used for expression studies are: Fig 1a, 1c, Extended Data Fig. 1f-i, Extended Data Fig. 2, Extended Data Fig. 3a-c, e,f - P10; Fig. 2a - P11; Fig 1b, Extended Data Fig. 1j, Extended Data Fig. 3d, g - P9; cDNA sequencing, P8. For entorhinal cortex tracing (Fig. 1d-e) animals were between P55 and P70 when perfused. For developmental tracing CD-1 animals were injected at P0 and perfused at P2, P4, P6, or P8. Ten3-Cre and Ten3-flox animals were on a mixture of CD-1, C57BL/6, and 129 backgrounds, and Ten3-delta4 was on a CD-1 background. For electrophysiology, animals were P14-P19, both sexes used. For tracing experiments in Ten3 mutants, animals were between P30 and P45 at the time of injection, and both sexes were used.

Policy information about studies involving human research participants

12. Description of human research participants

| | |
|---|---|
| Describe the covariate-relevant population characteristics of the human research participants. | The study did not involve human participants. |